

Final Technical Report

Project title

A Loss Estimation and Decision-Making Tool for Managing Fire Following Earthquake

Award number

USGS G19AP00055

Authors

Negar Elhami-Khorasani

Assistant Professor

136 Ketter Hall, Department of Civil, Structural and Environmental Engineering

University at Buffalo

Buffalo, NY, 14260

T: (716) 645 3019 F: (716) 645 3733 negarkho@buffalo.edu

Amir Sarreshtehdari

Ph.D. Candidate

206 Ketter Hall, Department of Civil, Structural and Environmental Engineering

University at Buffalo

Buffalo, NY, 14260

amirsarr@buffalo.edu

Project start date: June 2019

Project end date: May 2020

(a) Acknowledgement of support

This material is based upon work supported by the U.S. Geological Survey under Grant No. G19AP00055. Computational support was provided by the Center for Computational Research at the University at Buffalo (Center for Computational Research, 2020).

(b) Disclaimer

The views and conclusions contained in this document are those of the authors and should not be interpreted as representing the opinions or policies of the U.S. Geological Survey. Mention of trade names or commercial products does not constitute their endorsement by the U.S. Geological Survey.

Abstract

Historic events, such as the 1994 Northridge earthquake, confirm the risk of fire following earthquake (FFE) and how the likelihood of fire ignitions and potential for fire spread after an earthquake increases within a community. The recent study by the USGS on the HayWired earthquake scenario indicated that the fires following the main shock “would be directly responsible for the loss of hundreds of lives, a total building replacement value of almost \$16 billion, and total property losses approaching \$30 billion.” Evaluating performance of a community subjected to FFE involves a great level of uncertainty and depends on the behavior of buildings, bridges, roadways, water and electric networks, fire department resources, and their interaction. This project develops a loss estimation and decision-making framework for managing FFE, with the following two primary contributions:(a) establishing a model to assess fire department response to locations of ignition based on level of damage to the community after an earthquake, and available firefighting resources, (b) reducing uncertainty in predicting losses from FFE by integrating ignition, spread, and suppression phases with explicit consideration of fire department response. Performance of the transportation network is captured by inclusion of damage to bridges and generated debris from buildings on the roadways. Analysis of water network is performed while including damage to the network components and considering dependency of the network on electricity. Fire spread between and within buildings is incorporated in the framework. A decision-making algorithm is developed to assign fire engines to locations of ignition while minimizing the induced losses. The optimization process takes into account changes in response time of the fire department to locations of ignition, water availability, and appraised value of buildings. The developed framework is applied to a case study, demonstrating how different locations of ignition and level of damage to the infrastructure influences the potential for successful control of fire and consequently the associated losses. The results of this research can be used to develop action plans for preparedness, mitigation, and response of communities to FFE, including fire department resource allocation.

Contents

| | |
|--|----|
| (a) Acknowledgement of support..... | 2 |
| (b) Disclaimer..... | 2 |
| Abstract | 3 |
| 1 Introduction | 5 |
| 2 Transportation network | 7 |
| 2.1 Bridge functionality | 7 |
| 2.2 Roadway accessibility..... | 9 |
| 2.3 Transportation network analysis..... | 10 |
| 3 Water and electric networks..... | 11 |
| 3.1 Electric network..... | 11 |
| 3.2 Water network and dependency on power..... | 13 |
| 4 Ignition model | 14 |
| 5 Fire spread model | 14 |
| 5.1 Building-to-building fire spread | 14 |
| 5.1.1 Radiation | 14 |
| 5.1.2 Fire plume..... | 15 |
| 5.1.3 Fire branding | 16 |
| 5.1.4 Direct flame contact | 17 |
| 5.1.5 Piloted and spontaneous ignition..... | 17 |
| 5.1.6 Fire behavior inside a compartment | 17 |
| 5.2 Fire spread inside a building..... | 18 |
| 6 Suppression | 19 |
| 6.1 Required water to extinguish fire..... | 19 |
| 6.2 Time to extinguish fire..... | 20 |
| 7 Decision-making algorithm for assignment of fire engines | 22 |
| 7.1 Objective function..... | 23 |
| 7.2 Implementation of the objective function..... | 24 |
| 8 Application to a case study..... | 24 |
| 9 Conclusions | 31 |
| 10 Presentations and publications | 31 |
| 11 Project data..... | 31 |
| 12 References | 31 |

1 Introduction

Modern communities have been evolved to have interconnected social, economic, and infrastructure networks. Such interconnectivity between different parts of a system means failure in physical or organizational structure of a community can lead to cascading failures in other structures. In case of a hazard, an extreme event may cause direct infrastructure and asset losses, while the subsequent cascading damage due to disrupted operations can exceed the direct losses (Hay et al., 2014). If a city has to stay functional after a hazard and recover from the event, performance of individual critical structures, connectivity of infrastructure in the system, and the cascading effects on the system should be incorporated in the design, mitigation, and response planning. Earthquake is a potential hazard for communities located in seismically active regions, and fire following earthquake (FFE), a cascading multi-hazard event, can cause major social and economic losses in a community.

The likelihood of a fire event is typically amplified following seismic events mainly due to ruptured utility lines or toppled appliances. In addition, firefighter intervention can be hampered due to (1) loss of water pressure and flow as a result of ruptured water lines, widespread firefighting efforts, or loss of electricity at water pumping stations, and (2) inaccessible roadways as a result of damaged bridges, roadways, and debris. Thus, consequences of fire ignitions after an earthquake, if not controlled in time, could be disastrous, especially in highly populated urban areas (Taylor, 2003; Li and Davidson, 2013; Elhami Khorasani and Garlock, 2017).

Elhami-Khorasani and Garlock (2017) reviewed previous FFE events from seven countries with the majority of them occurring between 1971 and 2014, and confirmed that post-earthquake fire ignitions may cause considerable damage, and generally, chaos following an earthquake lowers the response time and resources of firefighters. Season (e.g., wind condition) and time of the day also play an important role on the rate of fire spread, while adequate water supply is key to control fire ignitions and spread. As an example, there were approximately 110 earthquake-related fires following the 1994 Northridge earthquake with a magnitude of 6.7 (Scawthorn et al., 2005). The earthquake caused significant damage to the Los Angeles water system including water supply and transmission systems (Davis et al., 2012). Loss of electric power in the Van Norman complex, that lasted about 24 hours after the earthquake, interrupted service in the largest water pumping station in the city system (O'Rourke, 2007). The firefighters had to use water from swimming pools as a back-up source of water to extinguish fires. After studying impacts of the 2014 South Napa earthquake, one of the priority recommendations was related to water supplies for firefighters. The recommendation was made due to potential vulnerability of water systems and the highlighted finding on “the additional fire hazards that earthquake-related water-system failures can pose [...]” (Johnson and Mahin, 2016). These FFE events are not limited to the US, , the Great East-Japan Earthquake of 2011, for example, was followed by substantial induced fire damage, which was “equivalent or even larger in size and diversity” compared to the 1995 Kobe earthquake in Japan (Scawthorn et al., 2005).

The recent study by the USGS on the HayWired earthquake scenario (USGS, 2018) indicated that fires following the main shock “would be directly responsible for the loss of hundreds of lives, a total building replacement value of almost \$16 billion, and total property losses approaching \$30 billion.” The Shakeout Scenario (Scawthorn, 2008) investigated the effects of a hypothetical 7.8 magnitude earthquake that occurred on the southern San Andreas Fault at 12 PM of a breezy day with relatively low humidity in the month of November. It was reported that such an earthquake could cause approximately 1600 fire ignitions, out of which 1200 would spread over large areas, and a few will grow into conflagrations. Another study conducted by the New York City Area Consortium for Earthquake Loss Mitigation (NYCEM, 2003) showed that a moderate earthquake could result in an estimated 1100-1200 deaths, and ignitions up to 900 fires simultaneously in the NY-NJ-CT area. Scawthorn (2019) completed a study on potential losses from FFE in Montreal, Canada, and estimated induced losses in the range of \$10 to \$30 billion under seismic scenarios with magnitudes 6.5 and 7. The study simulated 300 to 400 locations of ignition in the community.

Several studies have been conducted to model the three primary phases of FFE: fire ignition, fire spread,

and fire suppression (Scawthorn et al., 1981, 1985; Himoto and Tanaka, 2002; Otake et al., 2003; Iwami et al., 2004; Nussle et al., 2004; Ohgai et al., 2004; Himoto and Tanaka, 2005; Scawthorn et al., 2005; Davidson, 2009; Lee and Davidson, 2010a; Lee and Davidson, 2010b; Zhao, 2010; Himoto and Tanaka, 2012; Li and Davidson, 2013; FEMA, 2014; MAEVis, 2014; Rafi et al., 2018; Farshadmanesh and Mohammadi, 2019).

There are also two available programs for economic loss estimation with a capability to perform FFE analysis, Hazus (FEMA, 2014) and MAEVis (MAEVis, 2014). HAZUS is a GIS-based software, developed by the Federal Emergency Management Agency (FEMA), where the FFE module covers all three phases of fire ignition, spread, and suppression. MAEVis is an open-source platform for earthquake hazard risk management developed by the Mid-America Earthquake Center at the UIUC. The implemented FFE module in MAEVis focuses on the ignition phase, and is based on the post-earthquake ignition vulnerability of a region in Turkey (Yildiz and Karaman, 2013). The existing frameworks and tools make simplifying assumptions on modeling the suppression actions and can be improved to incorporate (1) effects of earthquake damage to water supply systems, (2) road accessibility for firefighting operations, and (3) allocation of firefighters to fire.

This project explicitly models layers of infrastructure, including buildings, transportation, electric and water networks and simulates the three phases of FFE (ignition, spread, and suppression) as stochastic processes. Figure 1 provides a schematic overview of modeling different layers of information and their relationship. Response time of the fire department is related to damage to critical bridges in the region, and debris accumulation on the roadways. At the same time, availability of water flow and pressure at the location of fire is taken into account. A decision-making algorithm is developed and implemented to minimize losses by prioritizing the order of fire engine assignments to the locations of ignition with constraints based on the number of fire engines, water flow and pressure availability, and roadway accessibility. The developed framework contributes practical knowledge for informed decision-making related to mitigation, preparedness, and response of communities to earthquake events.

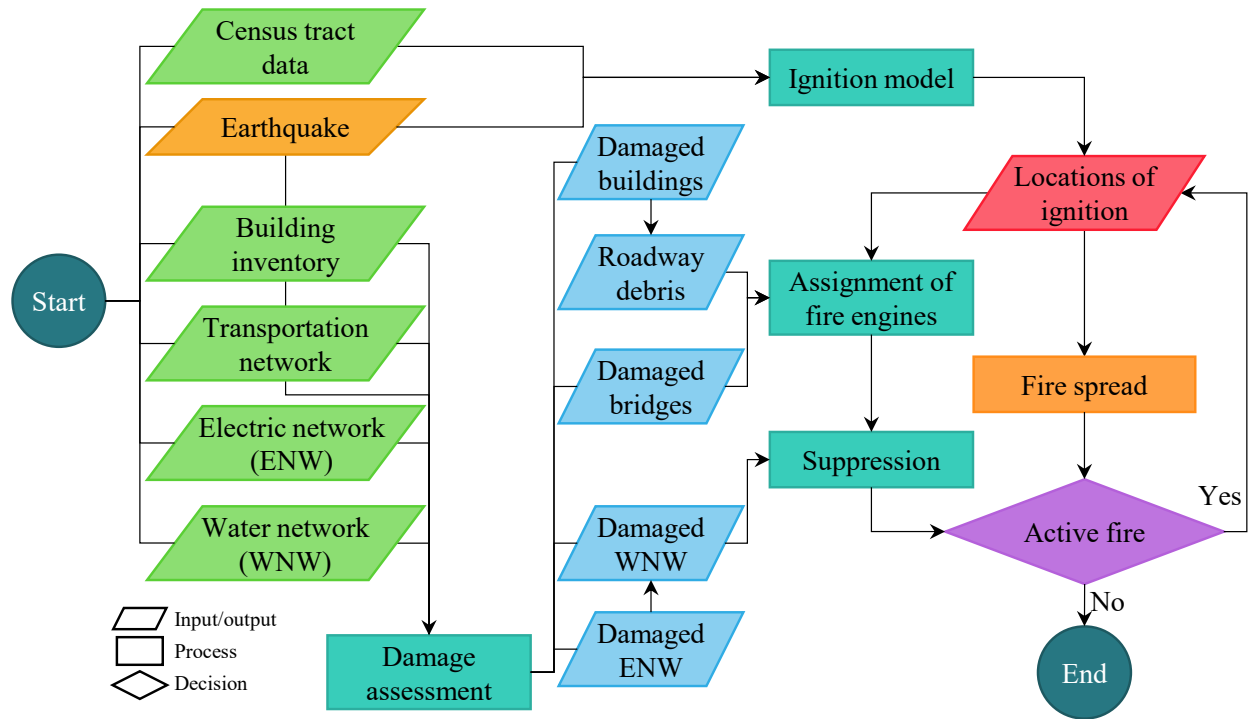


Figure 1: Schematic overview of the considered layers of information to model FFE losses

The following sections of this report provide a review of modeling approach for transportation network (Section 2), water and electric networks (Section 3), fire ignitions (Section 4), fire spread (Section 5), suppression actions (Section 6), and assignment of fire engines to minimize losses (Section 7). Results of model application to a case study is presented in Section 8.

2 Transportation network

Seismic damage to elements of the transportation network and debris from buildings could hamper the suppression process by firefighters. The transportation network, as a critical infrastructure system, comprise of roadways and bridges in the area. Depending on the layout of roadways, number and type of bridges, and the level of connectivity or redundancy in the network, damage to bridges or roadways could limit access to an area or result in complete inaccessibility. This section will discuss post-earthquake response time of the firefighters to locations of ignition.

2.1 Bridge functionality

Bridges, as a major component of the US transportation network, play a crucial role in connectivity of a community for post disaster response and allocation of resources. Induced damage and degradation in functionality level of bridges can be quantified utilizing fragility functions. Fragility functions quantify performance level of a component or system (e.g., bridge piers) by identifying the likelihood of exceeding a certain damage state given the intensity level of the earthquake. Fragility functions are generally represented by a lognormal distribution function, as shown in Eq. 1.

$$F(x)=P(LS | IM= im)=P(DS > ds | IM= im)= \Phi \left[\frac{\ln \left(\frac{x}{\mu} \right)}{\beta} \right] \quad \text{Eq. 1}$$

where a limit state (*LS*) is defined as the state for which the damage state (*DS*) exceeds the specified threshold *ds*, and when intensity measure (*IM*) reaches the values of *im*. The parameters μ and β are median and dispersion for the corresponding lognormal distribution. Given a system or component, the damage state thresholds (*ds*) are defined to represent different operability levels. The link between an individual damage state and performance of the structure is constructed using the Engineering Demand Parameter (*EDP*), which is an appropriate response quantity, such as drift, to estimate damage. The intensity measure (*IM*) should be selected in such a way to reflect the true behavior of the structure under study.

Given the large number of available bridge types, and the uncertainties in definition of damage states and derivation approaches of fragility functions, identifying proper fragility function parameters that would accurately reflect a bridge performance requires an extra amount of care. Therefore, a comprehensive literature review was conducted to collect, organize, and classify available bridge fragility functions, with the goal of minimizing the uncertainties in characterizing bridge performance given its type and physical characteristics. A bridge taxonomy was defined based on seismic demand (considering region, soil type, liquefaction, near or far from fault), superstructure characteristics (considering seismic design, girder type, material type, girder joint type, geometry, retrofit history) and substructure characteristics (considering the number of columns in bridge piers, abutment, retrofit history, and environmental exposure). This project collected and classified 182 sets of fragility functions for concrete and prestressed concrete bridges, and 88 sets of fragility functions for steel bridges. The collected data are compiled in a tool with an appropriate user interface (Figure 2) to sort, visualize, and select relevant fragility functions for the community under study. Details of the taxonomy and the collected database are provided in Sarreshtehdari and Elhami-Khorasani (2020).

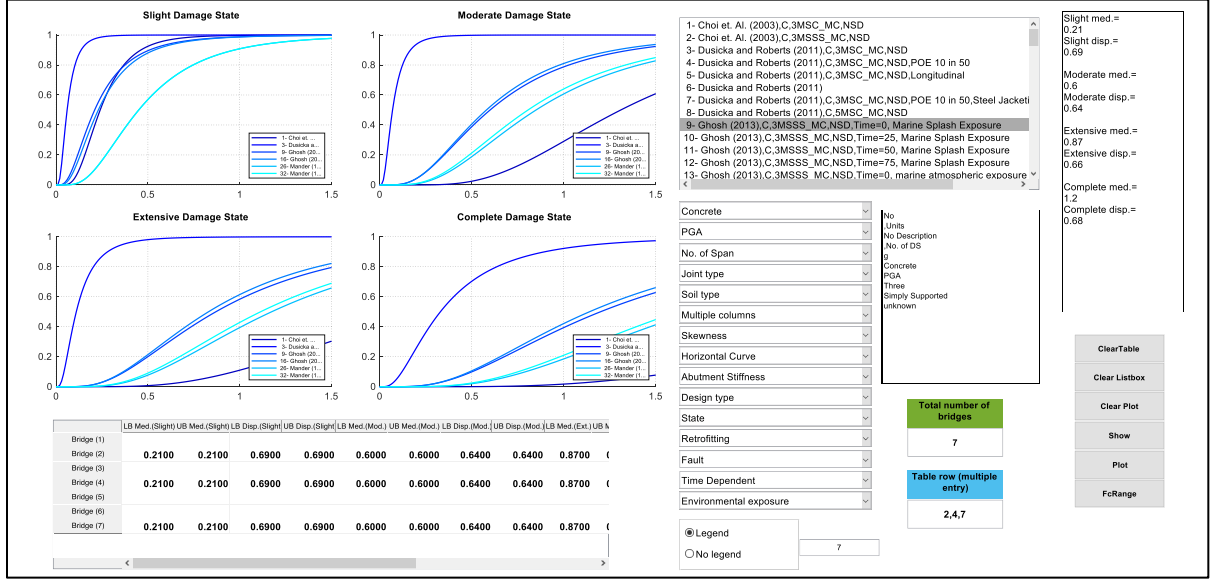


Figure 2: Snapshot of the user interface for the developed tool to access bridge fragility function database

A careful study of fragility function database shows a relatively large variation in fragility parameters of some bridge classes, which are obtained from different studies and are based on different methodologies. In order to incorporate such variations in the framework, an aggregation scheme was utilized to combine the available knowledge and randomly generate values for the median and dispersion of fragility functions. Figure 3 shows an example on parameter sampling of moderate (μ_i, β_i) damage state (μ_j, β_j), where each realization is picked randomly using Latin Hypercube Sampling (LHS) and assuming a uniform distribution for the random parameters. Each parameter has a range that is obtained from the collected fragility functions from the literature (Figure 3 shows an example for a non-seismic simply supported steel bridge class). The sampling process is setup to ensure (1) the median value for a given damage state does not exceed that of a higher damage state (e.g., a slight damage state should have a smaller median compared to moderate, extensive, and complete damage states), and (2) the probability of exceedance for a given damage state is greater than that of higher damage states (e.g., probability of exceeding slight damage state should be larger than moderate, extensive and complete damage states).

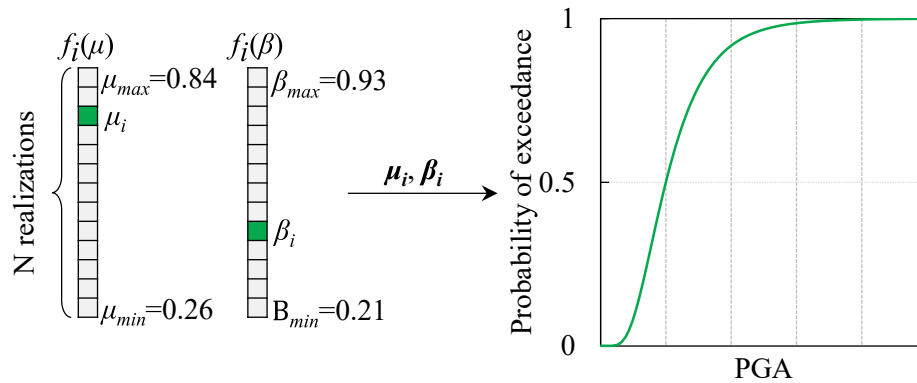


Figure 3: Sampling process for fragility function parameters of a moderate damage state (ds_i) for a non-seismic simply supported steel bridge class

In this study, the following categories of damage states are included: no damage, slight, moderate, extensive, and complete damage. For a given level of ground motion intensity, the probability of reaching different damage states are available. A random number between zero and one is generated and compared with the probability brackets for the damage states obtained from fragility functions. The bridge damage state is determined based on the bracket in which the randomly generated value lands. For example, the bracket for probability of slight damage state at lower *PGA* values covers a relatively large range, while this range narrows down at larger *PGA* values, as the probability of extensive or complete damage increases. The implemented process is validated using the 1994 Northridge earthquake as a case study. Figure 4 shows the area under study and the predicted damage states using the collected database of fragility functions and the methodology implemented in this work, in comparison to the reported damage states in the reconnaissance report after the earthquake (Basoz and Kiremidjian, 1998). The results provide a conservative quantification of damage, given the level of uncertainty involved in the process.

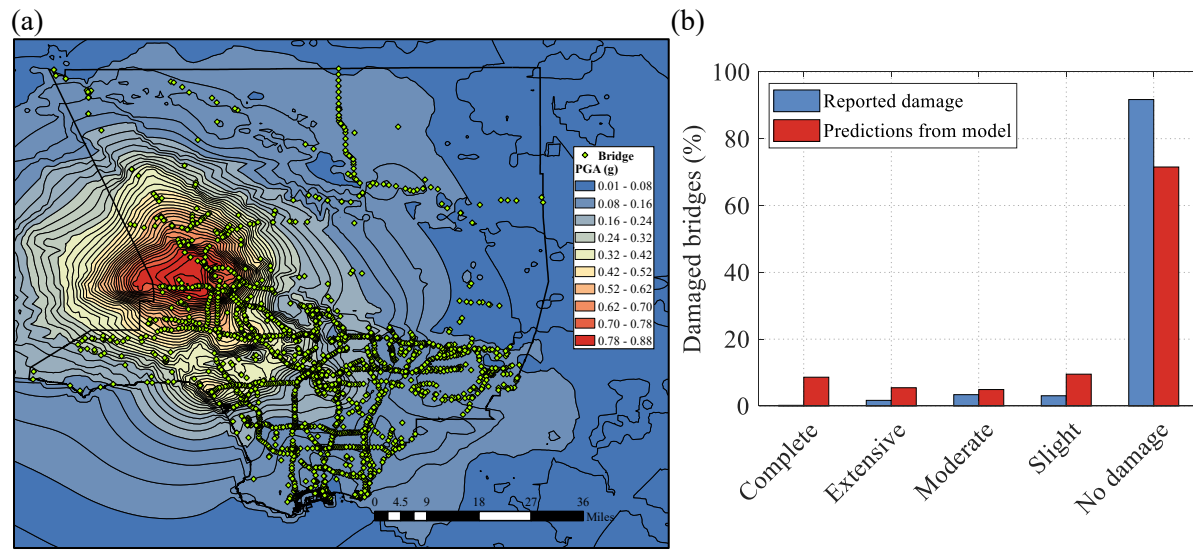


Figure 4: Northridge earthquake case study, (a) ShakeMap of the Los Angeles county with *PGA* values and locations of bridges, (b) comparison of reported damage states for bridges with model results

Finally, each damage state is mapped to a bridge functionality level (C_{bridge}), defined as whether a fire truck can cross the bridge or not. The bridge is assumed to be functional when it is classified under no damage, slight, or moderate damage categories, and non-functional in cases of extensive and complete damage states (Eq. 2).

$$C_{bridge} = \begin{cases} 1 & \text{functional} \\ 0 & \text{non-functional} \end{cases} \quad \text{Eq. 2}$$

2.2 Roadway accessibility

Potential roadway blockage due to building debris and traffic demand after an earthquake can affect the response time of the fire departments to the locations of ignition. This study only considers the effect of building debris on roadway accessibility, assuming that the fire department response is not significantly affected by other traffic on the roadways. The functionality level of roadways is defined by comparing the width of a roadway with the covering building debris width, including the curb distances. The methodology considers three most probable generated debris schemes from buildings based on historical incidents (Argyroudis et al., 2015). Figure 5 shows the three schemes and the width of generated debris based on building dimensions.

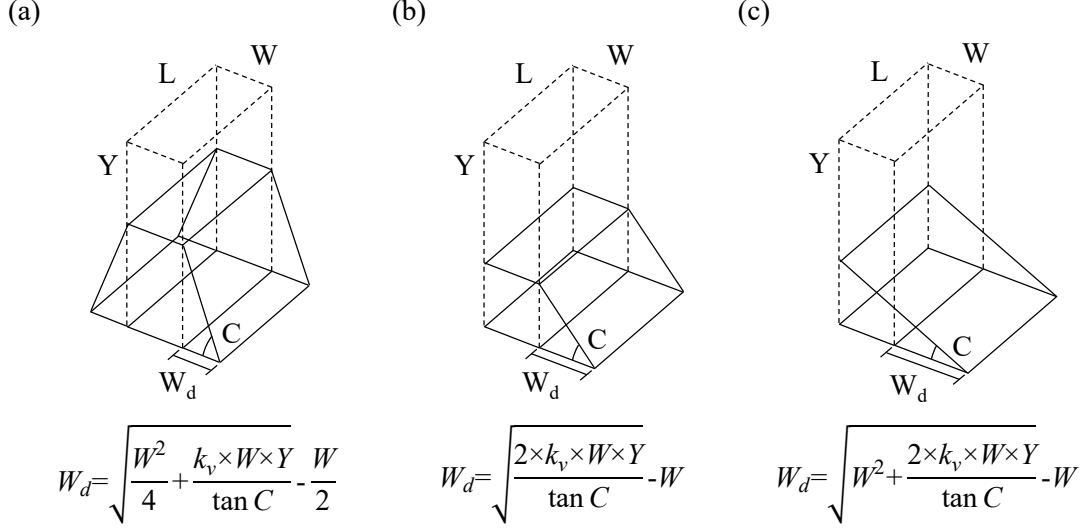


Figure 5: Three common debris generation schemes with the corresponding width

Factor k_v represents the debris volume fraction obtained by Eq. 3, where, k_p is the ratio of densities of the intact building to the generated debris, and k_m is the ratio of debris mass to the total building mass. The density of debris is estimated as 664.5 kg/m^3 (0.5 ton/yd^3). Hazus (FEMA, 2014) reports the unit weight of structural and nonstructural components per square footage of intact buildings, and lists fragility functions on the percentage of debris generated out of the total building weight, which can be related to building dimensions to calculate k_p . Detailed mathematical derivation to calculate the amount of debris as a function of k_p and k_m , is presented in (Sarreshtehdari and Elhami-Khorasani, 2020).

$$k_v = \frac{V_{debris}}{V_{initial}} = k_m \times k_p \quad \text{Eq. 3}$$

The three assumed schemes in Figure 5 are assigned randomly, with equal weights, to the buildings in the study area. Comparison of the generated debris width and the roadway width (including the curb distance) provides a measure of the roadway functionality level (C_{debris}) as defined in Eq. 4.

$$C_{debris} = \begin{cases} 1 & W_d < curb \\ 0.5 & curb \leq W_d < curb + \left(\frac{W_r}{2}\right) - W_F \\ 0 & curb + \left(\frac{W_r}{2}\right) - W_F \leq W_d \end{cases} \quad \text{Eq. 4}$$

where W_d is the debris width, *curb* is the distance from the building to the side of roadway, W_r is the width of roadway, and W_F is the width of a fire truck, with a typical value of 3 m (10 ft).

2.3 Transportation network analysis

As mentioned in Section 2.2, dynamic traffic assignment and traffic patterns after an earthquake are not considered in this study, especially due to lack of systematic historical data and level of uncertainty. The travel time of the fire engines from the fire station (or any other starting position in the community) to the location of ignition (i.e., destination) is calculated by construction the transportation network and using the shortest-path algorithm by Dijkstra (1959). The travel time, calculated as the length of roadway divided by the speed limit, is assigned as the weight of each link (roadway or bridge) in the constructed graph of the transportation network. The effect of degradation in functionality level, to arrive at the damaged travel time

($t_{damaged}$), is incorporated by applying a capacity reduction factor (C_{DS}) to the intact travel time (t_{intact}) using Eq. 5. Parameter C_{DS} is replaced by C_{bridge} or C_{debris} (from Eqs. Eq. 2 and Eq. 4) depending on the link type.

$$t_{damaged} = \frac{t_{intact}}{C_{DS}} \quad \text{Eq. 5}$$

3 Water and electric networks

When fire engines reach the locations of ignition, sufficient water flow and pressure are key for a successful suppression action. The water network may suffer damage during the earthquake. In addition, operation of water pumps can be compromised due to damage in the electric network. Historical events confirm the dependency of water network on power (Anshel, 1985; Schiff, 1998; Botting, 1998; Wellington Lifelines Group, 2002; Davis et al., 2012; DOE, 2013). Performance of water and electric networks after an earthquake and their dependency has been investigated by a number of studies (Dueñas-Osorio et al., 2007; Adachi and Ellingwood, 2008; Shi and O'Rourke, 2008; Franchin, 2014; Johnson and Tien, 2018). Generally, the overall performance of a network can be quantified either by topological metrics or explicit flow-based analysis. Topological characteristics of a network can provide an overall assessment of the network performance, which is useful for comparison of functionality before and after an earthquake. However, topological metrics cannot necessarily capture the detailed behavior of the network and at times, do not take physics of the problem into account.

In this project, water and electric networks are analyzed using graph theory, and their performance is evaluated using flow network analysis. A graph consists of vertices, which are connected with edges (Deo, 1974). Here, vertices in the network are categorized into (1) source vertices which generate input flow to the system, (2) sink vertices which determine the demand, and (3) intermediate vertices connecting the source and sink vertices. The following sections discuss the implemented methodology for system level analysis of water and electric networks and their dependency.

3.1 Electric network

Electric network is analyzed using flow network analysis, where power plants are modeled as source vertices, substations as sink vertices, and transmission lines as intermediate vertices. The amount of flow in the electric network is solved using the directed maximum flow analysis where multiple source and sink vertices are transformed to a single virtual source and a single virtual sink (Boykov and Kolmogorov, 2004; Atkins, 2009). The maximum flow is a graph-based approach, with the goal of maximizing flow from the source to the sink, while limiting the maximum amount of flow passing through an edge considering its capacity. Directed flow analysis enforces a predefined direction of the flow (from sources to the sinks in this case).

Hazus (FEMA, 2014) classifies power plants based on their output capacity, where small power plants have a capacity of less than 200 MW, and medium/large power plants have capacity levels greater than 200 MW. Substations are classified as low, medium, and high voltage according to their maximum voltage of 115 kV, 230 kV and 500 kV, respectively (FEMA, 2014). The transmission lines distribute the electricity across the network and connect individual system components. The transmission lines are also classified based on voltage, including low voltage (less than 30 kV), medium voltage (between 30 and 150 kV), and high voltage (from 220 up to 500 kV). Power plans and substations may experience damage during an earthquake. The level of damage for these components is quantified using fragility functions, with parameters taken from Hazus (FEMA, 2014), and as listed in Table 1 and Table 2. Shinozuka et al. (2004) and Yang et al. (2017) demonstrated that, among the main components of an electric network, transmission lines are not susceptible to seismic damage.

Table 1: Fragility parameters for different classes of power plants

| Damage state | Small generator | | Medium/large generator | |
|--------------|-----------------|---------|------------------------|---------|
| | Median | β | Median | β |
| Slight | 0.10 | 0.55 | 0.10 | 0.60 |
| Moderate | 0.21 | 0.55 | 0.25 | 0.60 |
| Extensive | 0.48 | 0.50 | 0.52 | 0.55 |
| Complete | 0.78 | 0.50 | 0.92 | 0.55 |

Table 2: Fragility parameters for different classes of substations

| Damage state | Low voltage | | Medium voltage | | High voltage | |
|--------------|-------------|---------|----------------|---------|--------------|---------|
| | Median (g) | β | Median (g) | β | Median (g) | β |
| Slight | 0.15 | 0.70 | 0.15 | 0.60 | 0.11 | 0.50 |
| Moderate | 0.29 | 0.55 | 0.25 | 0.50 | 0.15 | 0.45 |
| Extensive | 0.45 | 0.45 | 0.35 | 0.40 | 0.20 | 0.35 |
| Complete | 0.90 | 0.45 | 0.70 | 0.40 | 0.47 | 0.40 |

Given the earthquake intensity, a capacity index is defined to aggregate and map the information from probabilities of having different damage states to the level of functionality, as shown in Eq. 6 (Bai et al., 2009; Sarreshtehdari et al., 2020).

$$C = \sum_{i=1}^{n+1} c_i p_i \text{ where } p_i = P_i - P_{i-1} \quad \text{Eq. 6}$$

In the above equation, n is the number of damage states, c_i is the assumed remaining capacity for damage state i , p_i is the probability of occurrence of damage state i , which is calculated as the difference of probabilities of exceeding damage states i (P_i) and $i-1$ (P_{i-1}). The value of c_i ranges from 0.0, for complete damage, and 1.0, for the case of no damage. Sarreshtehdari et al. (2020) calibrated the c_i values for intermediate damage states based on the reported operability level of electric network components during the 1995 Kobe earthquake (Shinozuka, 1995). Table 3 provides the proposed values for the c_i for power plants and substations.

Table 3: Proposed values for capacity level c_i as a function of damage state

| Damage state | Complete | Extensive | Moderate | Slight | No damage |
|--------------|----------|-----------|----------|--------|-----------|
| c_i | 0.0 | 0.58 | 0.76 | 0.89 | 1.0 |

Once the capacity of power plants and substations are adjusted based on the earthquake intensity, the maximum flow analysis can be completed to solve for the flow in the network. In order to determine if a substation is operational or not, a ratio is defined to compare the flow, in each vertex, before and after the earthquake, as shown in Eq. 7:

$$\begin{cases} \text{if } \frac{f_{dmg}}{f_{intact}} \geq \alpha, & \text{component is operable (i.e., bright)} \\ \text{if } \frac{f_{dmg}}{f_{intact}} < \alpha, & \text{component is inoperable (i.e., dark)} \end{cases} \quad \text{Eq. 7}$$

where f_{dmg} is flow in the damaged condition, f_{intact} is flow in the intact condition, and α is a defined threshold to distinguish between an operable (i.e., bright) and inoperable (i.e., dark) substation. The value of α is set to 0.5. The methodology was validated (details discussed in Sarreshtehdari et al., 2020) using the two case studies of the Los Angeles Department of Water and Power (LADWP) after the 1994 Northridge earthquake (Shinozuka et al., 2004), and the electric network located in Shelby County in the New Madrid seismic zone (Shinozuka et al., 1998).

3.2 Water network and dependency on power

Components of a water network include tanks, reservoirs, and water treatment plants as sources of water flow, pipes as the distribution lines, and pumps to provide sufficient pressure for the designated service area. Graph of the water network is constructed similar to the electric network. Hazus (FEMA, 2014) lists the parameters of relevant fragility functions for different components, and based on their size and seismic design. Earthquake damage to components is quantified using the capacity index as defined in Eq. 6. The water head (i.e., pressure) and flow in the network are evaluated using the gradient method in conjunction with the pressure-deficient network algorithm (PDNA) (Boulos et al., 2006; Coar et al., 2020), which is based on the principle of conservation of energy along the pipes, with the Hazen-Williams frictional constant and conservation of mass (flow) in pipe joints. The PDNA algorithm prevents solutions with negative pressure in demand nodes by replacing pressure deficient nodes with artificial reservoirs. When solving the system for FFE application, a minimum water pressure of 14 m (20 psi) is required at any given fire hydrant during fire suppression activity.

Functionality of pumps, as a power-dependent component, depends on the level of earthquake damage to the pump facility, as well as availability of power. Coar et al. (2020) compared the operability level of nodes in a water network considering three different scenarios: (1) no dependency to power, (2) implicit modeling of power dependency, and (3) explicit modeling of power dependency. The first approach ignored potential degradation in water pressure and flow due to power outage. The implicit approach introduced dependency of a pump station on power by adding a sub-component branch related to power in the logic fault tree when constructing the fragility function of the component (Alexoudi et al., 2010; FEMA, 2014). This way, the probability of exceeding the damage state ds for a pump station $P(ds|PGA)$ is calculated as a function of fragilities for each subcomponent SC_i (including damage to the pump building, equipment, tank, and power), as shown in Eq. 8:

$$P(ds|PGA) = 1 - \prod_{i=1}^n (1 - P_{SC_i}(ds|PGA)) \quad \text{Eq. 8}$$

where $P_{SC_i}(ds|PGA)$ is the fragility function of pump subcomponents for the damage state ds given the earthquake PGA .

The explicit modeling of dependency relies on electric network analysis as discussed in the previous section. If a pump station is located within the service area of a dark power substation, the component is not operational. In the case of a bright substation, the component is operational at a level of damage induced from the earthquake. Coar et al. (2020) concluded that, when significant amount of system's total pressure depends on electrically powered sources, explicit analysis shows significant operability reduction compared to implicit and no dependency analysis. At higher earthquake intensities, ignoring explicit dependency of the water network on power may provide inaccurate and unconservative predictions of available water pressure at fire hydrants. In this work, dependency of water network on power is addressed considering the explicit approach.

4 Ignition model

The number of ignitions following an earthquake are estimated using a data-driven model by Elhami-Khorasani et al. (2017). This model is based on compiled data from historical FFE incidents in California between 1983 to 2014. The probability of ignition in a census tract is related to seismic intensity, population density (PD), and total square footage of the buildings (SF). Given probability of ignition in a census tract, the probability of ignition in a building is calculated based on the construction type, which is then used to estimate the number of ignitions for a given census tract. To use the model, one compiles an inventory of census tracts for the region of study including population density (PD), total square footage of the buildings (SF), number of wood buildings (N_W), number of mobile homes (N_{MH}), and number of non-combustible buildings (N_{NC}). Eq. 9 is used to calculate the probability of ignition in a census tract given the characteristics of the community and the PGA values. Having the probability of ignition in each census tract and the number of each building type, probability of ignition (P_{Ig}) for each building type can be calculated from the relationship in Eq. 10. Finally, the expected number of ignitions (N_{Ig}) in “ m ” census tracts equals to the sum of probabilities of ignitions for all buildings in these census tracts, shown in Eq. 11.

$$P_{Ig_tract} = \frac{\exp(-6.755 + 8.463 \times PGA + 98.4 \times 10^{-6} \times PD + 152.3 \times 10^{-6} \times SF)}{1 + \exp(-6.755 + 8.463 \times PGA + 98.4 \times 10^{-6} \times PD + 152.3 \times 10^{-6} \times SF)} \quad \text{Eq. 9}$$

$$P_{Ig_tract} = 1 - [(1 - 0.471 P_{Ig}) | PGA]^{N_W} \times [(1 - 1.0 P_{Ig}) | PGA]^{N_{MH}} \times [(1 - 0.411 P_{Ig}) | PGA]^{N_{NC}} \quad \text{Eq. 10}$$

$$N_{Ig} = \sum_{i=1}^m [N_W \times (0.471 P_{Ig}) + N_{MH} \times (1.0 P_{Ig}) + N_{NC} \times (0.411 P_{Ig})]_i \quad \text{Eq. 11}$$

5 Fire spread model

This section will discuss the implemented fire spread model to capture fire propagation from building to building and inside a building. The adapted framework takes the physics of the problem into account while relying on empirical relationships where the physics-based model is computationally too expensive or requires inputs with large uncertainties. The community layout, which is represented by a raster matrix, is discretized into $10 \text{ m} \times 10 \text{ m}$ cells, each cell representing a compartment with assigned characteristics (e.g., construction type, temperature-time evolution in case of a fire, etc.). In addition to a two-dimensional fire spread within the plan view of a community, which has been studied by others, building height is considered as an input to the fire spread model. Therefore, a three-dimensional mesh size of $10 \text{ m} \times 10 \text{ m} \times 3 \text{ m}$ is adapted to discretize the community. The fire spread model considers propagation from building to building and inside a building. Building-to-building fire spread is based on the physics of the problem, while spread within a building is captured using existing data and observations from traveling fire research in the literature.

5.1 Building-to-building fire spread

The developed framework in this study considers thermal radiation, fire plume, direct flame contact, and fire branding, while the two latter modes are applied to wood structures only.

5.1.1 Radiation

The thermal radiation flux \dot{q}'' (kW/m^2) at the receiver surface of a given fire compartment can be calculated as following:

$$\dot{q}'' = \sigma \epsilon \phi (T_e^4 - T_r^4) \quad \text{Eq. 12}$$

where σ is the Stefan-Boltzmann coefficient (5.67×10^{-11} kW/m²K⁴), ϵ is the emissivity of the emitter surface, ϕ is the configuration factor, T_e is temperature of the emitter surface (K), and T_r is temperature of the receiver surface (K). The configuration factor ϕ reflects the effect of geometry and distance on transmission of radiation from emitter to the receiver. The configuration factor can be simplified and conservatively calculated using Eq. 13, assuming the emitter and receiver surfaces are parallel. In Eq. 13, A_e is the area of the emitting surface, and r is the distance between the two surfaces. The model takes the emitter surface as the exterior surface of the emitter compartment and the receiver surface as a virtual surface located at the center of the receiver compartment.

$$\phi = \frac{A_e}{\pi r^2} \quad \text{Eq. 13}$$

The radiation sources from an emitter surface include gas temperature, ejected flames from windows, and heated walls. The implemented model follows the work of Himoto and Tanaka (2005) and calculates total radiation from the emitted compartment based on the average radiation emitted from the wall, openings, and ejected flames. According to Zhao (2010), the contribution of radiation from the flame and wall can be assumed as 20% of the total radiation. Geospatial assignment of compartments receiving radiation is tracked in the model. Receiver compartments include only those that are exposed to the source of radiation, in other words, the interior compartments of a building do not receive radiation. A ray casting algorithm is implemented to detect the visible compartments within a range of -90 to +90 degrees of the wind direction from a given fire source. Wind direction is a user specified input and can change at every time step of the simulation.

5.1.2 Fire plume

Turbulent fire plume increases temperature due to convective heat flow in downwind direction. The changes in temperature at the centerline of the plume follows a Gaussian distribution profile with the mean value from Eq. 14 (Beyler, 1986; Himoto and Tanaka, 2002).

$$\Delta T_m = \begin{cases} 900 \left(\frac{Z}{\dot{Q}^{2/5}} \right)^{-1} & \frac{Z}{\dot{Q}^{2/5}} < 0.08 \\ 60 \left(\frac{Z}{\dot{Q}^{2/5}} \right)^{-1} & 0.08 \leq \frac{Z}{\dot{Q}^{2/5}} < 0.2 \\ 24 \left(\frac{Z}{\dot{Q}^{2/5}} \right)^{-5/3} & 0.2 \leq \frac{Z}{\dot{Q}^{2/5}} \end{cases} \quad \text{Eq. 14}$$

where \dot{Q} is Heat Release Rate (HRR) of fire source (taken as the HRR of fire compartment), Z is distance from the fire source along the plume line, and ΔT_m is the temperature rise along the vertical plume center line. Verriopoulos and Papailiou (1998) proposed Eq. 15 to correlate plume temperature rise at radial distances with the centerline temperature:

$$\Delta T_{r,p} = \exp \left[- \ln 2 \left(\frac{r_p}{b_{0.5}} \right)^2 \right] \Delta T_m \quad \text{Eq. 15}$$

where $\Delta T_{r,p}$ is the temperature rise at the radial distance r_p (m) from the plume center line, and $b_{0.5}$ is the half-width Gaussian distribution in Eq. 16:

$$b_{0.5} = 0.132 D \left(\frac{Z}{D} + 3.6 \right) \quad \text{Eq. 16}$$

where D (m) is the width of fire source, here assumed as the square root of the fire compartment plan area. The abovementioned formulation considers only the vertical fire plume while the effect of wind is included according to Himoto and Tanaka (2002). The combined effects of temperature rise on a single receiver compartment, from multiple sources of fire plume, are quantified as:

$$\Delta T_T = \left[\sum_{i=1}^N (\Delta T_i)^{\frac{3}{2}} \right]^{\frac{2}{3}} \quad \text{Eq. 17}$$

where ΔT_i is the temperature rise by fire plume i and N is the total number of plume sources. The fire spread due to plume mechanism affects the same compartments as those identified by the ray casting algorithm for radiation. The induced convective heat flux due to temperature rise is calculated using the fundamental heat transfer equation for convection, with the convective heat transfer coefficient of $25 \text{ W/m}^2\text{K}$ (the typical range for a free flow application is between $5\text{-}25 \text{ W/m}^2\text{K}$ (Drysdale, 2011)).

5.1.3 Fire branding

Modeling fire spread due to branding includes three main stages: generation, transportation, and ignition. A number of studies relevant to different stages of fire branding as applied to construction material (rather than vegetation) have been completed: generation (Waterman, 1969), transportation (Woycheese et al., 1999; Anthenien et al., 2006; and Sardoy et al., 2007), and accumulation and ignition (Gol'dshleger et al., 1975). Branding is a major contributor to fire spread, especially for far field spread in areas with high concentration of wood buildings. Larger fire plume (vertical transport), higher wind velocities (horizontal transport), lower humidity, and higher vegetation densities magnify the effect of firebrands. In this study, generation of firebrands is modeled based on the works of Waterman (1969) and Lee and Davidson (2010), while transportation of firebrands is modeled following the work of Himoto and Tanaka (2005). The only contributing compartments, where firebrands can be generated, are those located at the top story of timber buildings.

The number of generated firebrands is calculated based on Waterman's experiments (1969). The experiments investigated the effects of typical roofing material and wind velocity on the generation of firebrands. Lee and Davidson (2010) proposed Eq. 18 to correlate the number of generated firebrands in Waterman's experiments with wind velocity.

$$N_b = 306.77 \exp [0.1879 U_\infty] \quad \text{Eq. 18}$$

where, U_∞ is the wind velocity (m/s) and N_b is the total number of generated firebrands per unit of area (m^2).

The implemented model for branding transportation predicts the landing locations stochastically according to a lognormal distribution in the downwind direction, with parameters shown in Eq. 19, and a normal distribution in the perpendicular direction, with parameters shown in Eq. 20. The model includes different aspect ratios and densities for the particles to take the material type of fire source into consideration.

$$\mu_x = 0.47 B_{brand}^{\frac{2}{3}} D, \sigma_x = 0.88 B_{brand}^{\frac{1}{3}} D \quad \text{Eq. 19}$$

$$\mu_y = 0, \sigma_y = 0.92 D \quad \text{Eq. 20}$$

where D is the width of fire source, taken as the square root of the fire compartment area, and B_{brand} is the non-dimensional parameter, calculated as:

$$B_{brand} = \left(\frac{U_{\infty}}{\sqrt{gD}} \right) \left(\frac{\rho_p d_p}{\rho_{\infty} D} \right)^{-\frac{3}{4}} \left(\frac{\dot{Q}}{\rho_{\infty} c_p T_{\infty} g^{\frac{1}{2}} D^{\frac{5}{2}}} \right)^{\frac{1}{2}} \quad \text{Eq. 21}$$

In the above equation, U_{∞} is the wind velocity (m/s), g is the gravitational acceleration (m/s^2), ρ_p is the density of firebrand particles (kg/m^3), d_p is the particle diameter (m), \dot{Q} is the HRR of fire compartment (kW), ρ_{∞} is the density of air with the value of $1.225 \text{ (kg/m}^3\text{)}$, c_p is the specific heat of ambient air with the value of 1.005 (kJ/kg K) , and T_{∞} is the ambient temperature of air (K). Table 4 lists the physical characteristics and proportions of different ember sizes during the transport process based on the work of Lee and Davidson (2010b) and collected data by Waterman (1969).

Table 4: Physical characteristics of embers

| Size | Brand area (cm^2) | Brand thickness (cm) | Brand density (kg/m^3) | Proportion (%) |
|--------|------------------------------|----------------------|-----------------------------------|----------------|
| Fine | 0.13-1.29 | 0.25-0.76 | 50-200 | 71 |
| Medium | 1.29-6.45 | 0.76-1.02 | 50-200 | 27 |
| Coarse | 6.45-58.06 | 1.02-1.78 | 50-200 | 2 |

5.1.4 Direct flame contact

The contribution of physical flame contact with the adjacent building is considered only for timber buildings (i.e., combustible material). The fire is assumed to spread to adjacent buildings or compartments when reaches a fully developed condition at a given compartment.

5.1.5 Piloted and spontaneous ignition

The occurrence of spontaneous ignition from radiation and convective heat flux is related to the exposure time to heat and material type of the receiver surface. Quintiere (2006) reports the time to ignition as a function of heat flux, based on experiments on different types of wood conducted by Spearpoint (1999) and Boonmee (2004), where increase in the received heat flux decreases the ignition time. The implemented model in this project assumes a critical heat flux of 30 kW/m^2 for spontaneous ignition of the receiver surface (Cousins et al., 2002). Delay time in case of piloted ignition is incorporated with respect to different heat flux values, where the compartment will be ignited in 5, 10 and 15 minutes when exposed to heat flux values greater than 20, 15 and 12.5 kW/m^2 , respectively. There is no established ignition criterion for fire branding, as it is a function of several parameters, such as material type of the receiver surface, humidity, layout of landed firebrands, etc. Thus, the ignition criteria for fire branding is modeled probabilistically, with probability of ignition due to firebrands assumed as 0.0, 0.005, and 0.020 for fine, medium, and coarse embers as defined in Table 4 (Waterman and Takata, 1969; Ohmiya and Owami, 2000; Lee and Davidson, 2010b).

5.1.6 Fire behavior inside a compartment

The evolution of fire inside a compartment, in the form of HRR and temperature, is required as an input to the fire spread model. Here, the evolution of fire is characterized using the parametric time-temperature and HRR curves of the Eurocode Annex E (Eurocode EN-1991, 2002). OZone (Cadorin and Franssen, 2003) is used to simulate fire scenarios for an office occupancy. Variability in the size of openings and fire area are taken into account based on listed values in Table 5, and assuming a uniform distribution for the random variables. A total of 625 scenarios (shown in Figure 6) are generated and randomly assigned to each building while keeping the same fire scenario for compartments in a given building.

Table 5: Considered range of inputs for fire scenarios in the OZone model

| Parameter | min | max | Sample size |
|-----------------------------|-----|-----|-------------|
| Opening sill height (m) | 0.5 | 1.0 | 5 |
| Opening soffit height (m) | 2.5 | 2.8 | 5 |
| Opening width (m) | 3.0 | 6.0 | 5 |
| Fire area (m ²) | 70 | 90 | 5 |

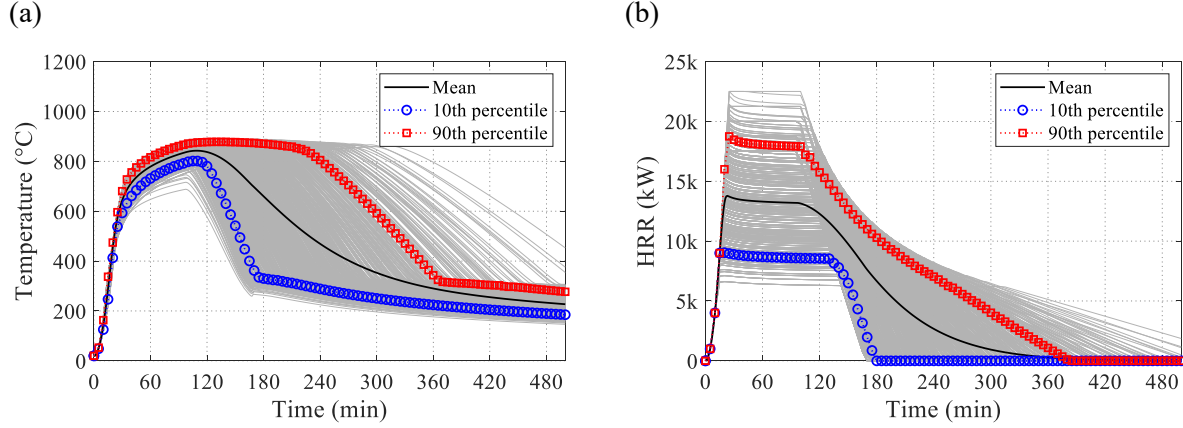


Figure 6: Generated (a) time temperature curves and (b) HRR curves for a 10×10×3 m fire compartment

5.2 Fire spread inside a building

Once a fire starts in a building, if it is not suppressed, it will spread within a floor and along the height of the structure. Different studies are looking into modeling traveling fires inside a structure (Rehm et al., 2003; McAllister et al., 2013). This process is simulated either by inducing a time delay between occurrence of fire in a given compartment and the corresponding adjacent compartments, or by explicitly modeling the rate of fire spread. Observations from historical incidents provide insight on the propagation of fire in horizontal and vertical directions. Bailey et al. (1996) assumed 36 minutes time delay between the ignition of two adjacent 8 m bays in a steel framed building. The horizontal fire spread rate in the Grenfell Tower fire incident was reported as approximately 0.3 meter per minute (Guillaume et al., 2020), which translates to 30 minutes time delay between two 10 m compartments. In case of vertical travelling fires, the major source of data are video recordings of fire incidents from outside of buildings. For example, the reported values of vertical fire spread time between floors in the 2005 Windsor Tower fire in Spain ranges from 6 to 15 minutes (Fletcher et al., 2006). Röben et al. (2010) and Rackauskaite et al. (2017) specified the travelling fire time delay between floors in the range of 8 to 25 minutes for fast and slow rates of fire spread, respectively. During the 1991 Meridian Plaza building fire in Philadelphia, Pennsylvania, the flames reached the 24th floor from the 22nd floor within an hour, caused by fire lapping out of side windows (FEMA, 1991). A rapid exterior fire spread of 3 minutes per floor was observed during the 2014 Lacrosse building in Melbourne, Australia (MFB, 2014), likely related to the façade type. Similarly, the Grenfell Tower in London experienced a vertical fire spread rate ranging from 1.7 to 3.6 meter per minute at different stages of fire due to usage of highly combustible material in the façade (Guillaume et al., 2020). The vertical fire spread phenomenon occurs mainly at the exterior surface of the building, but given the construction type and code regulations in the US, it is expected not to have highly combustible materials in current building façades and no such event has been recorded recently in the US.

Considering the fact that the compartmentation after an earthquake could be compromised (due to damage to partitions, walls, ceilings, etc.), and based on the above discussion, a horizontal fire spread rate of 30

minutes inside a building and a vertical fire spread rate of 10 minutes in the exterior compartments are assumed in this study.

6 Suppression

The suppressive action of firefighters on the rate of fire spread in an urban fire can be modeled using empirical or physics-based approaches. In either case, the flow rate of extinguishing agent (i.e., water for application in urban settings) is required as an input to the analysis. In this section, an overview of the minimum required water flow and the time to extinguish a fire are provided based on the governing energy equations of a two-zone model in a fire compartment. The model is based on conservation of energy within a control volume, where the rates of change in heat and ventilation within the control volume are taken into account.

6.1 Required water to extinguish fire

The governing energy equation for a two-zone model in a fire compartment, including losses from the absorbed energy by water and boundaries, has the following form (Quintiere, 2006):

$$\frac{d}{dt}(c_{p_{mix}}\rho_{mix}VT) = \dot{Q}_{fuel} - \dot{Q}_{water} - \dot{Q}_{loss} + (\dot{Q}_{in} - \dot{Q}_{out}) \quad \text{Eq. 22}$$

where $c_{p_{mix}}$ is the heat capacity of mixed gases in the control volume (kJ/kgK), ρ_{mix} is the density of mixed gases in the control volume (kg/m³), V is the volume of fire compartment (m³), T is the gas temperature in the control volume (K), \dot{Q}_{fuel} is the heat release rate of fire source (kJ/s), \dot{Q}_{water} is the rate of energy absorbed by water (kJ/s), \dot{Q}_{loss} is the rate of energy losses due to absorption by boundaries (kJ/s), and the last term on the right hand side of the equation is the rate of energy change due to ventilation (kJ/s). Figure 7 shows the schematic view of the assumed zone model, where variable H_o is the opening height (m) of the control volume. In this study, it is assumed that there is one horizontal opening in the fire compartment with no vertical ventilation in the ceiling.

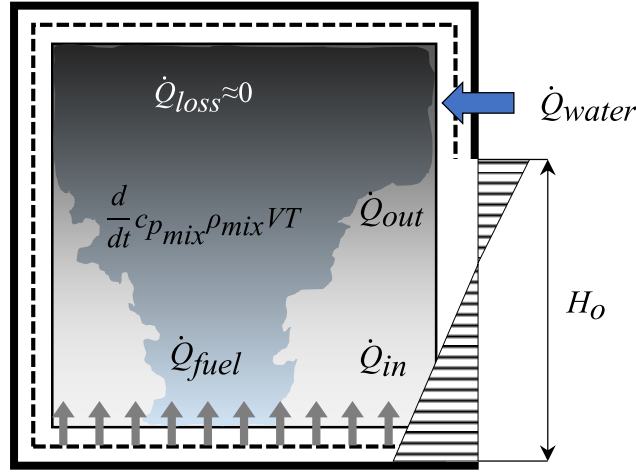


Figure 7: Zone model representation of a fire compartment, with contributing parameters to the governing equation of conservation of energy

The left side of Eq. 22 represents the rate of change in energy in the control volume. This term becomes zero under the steady-state condition, when the rate of change in temperature is negligible (Quintiere, 2006). Also, the same term becomes zero under the assumption of ideal gas with constant pressure within the control volume (Himoto and Tanaka, 2012). Note that assuming a steady state condition during a building fire is considered as an idealized assumption, in which the temperature in the compartment is uniform and

is independent of time (Tanaka, 2016). Therefore, Eq. 22 can be re-written as if an idealized steady state condition is reached and the rate of energy losses is neglected in order to simplify the governing energy equation. The factor ϕ_v is a coefficient to incorporate the level of efficiency in water discharge during suppression (Himoto and Tanaka, 2012). The lower cool layer of inflow \dot{Q}_{in} , and the upper hot outflow rate of enthalpy \dot{Q}_{out} in the control volume can be formulated following a two-zone model as described in (Quintiere, 2006).

$$\dot{Q}_{fuel} = \phi_v \dot{Q}_{water} - (\dot{Q}_{in} - \dot{Q}_{out}) \quad \text{Eq. 23}$$

The energy absorption rate of water in Eq. 23 can be formulated as:

$$\dot{Q}_{water} = \dot{m}_{water} c_w (T_{vapor} - T_{water}) + \dot{m}_{water} L_w \quad \text{Eq. 24}$$

where \dot{m}_{water} is the water flow rate in the compartment (kg/s), c_w is the heat capacity of water (kJ/kgK), T_{vapor} is the vaporization temperature of water, taken as 100°C (373 K), T_{water} is the temperature of water during suppression, taken as 20°C (293 K), L_w is the heat of gasification for water with the value of 2400 (kJ/kg). Combining Eq. 23 and Eq. 24, the required water discharge rate is quantified as:

$$\dot{m}_{water} = \frac{\dot{Q}_{fuel} + (\dot{Q}_{in} - \dot{Q}_{out})}{\phi_v (c_w (T_{vapor} - T_{water}) + L_w)} \quad \text{Eq. 25}$$

6.2 Time to extinguish fire

Extinguishing a fire changes the system from burning condition towards ambient condition. This section describes the procedure to characterize the time required to extinguish a fire based on the relevant physics of the processes, governing equations of the system, and the diffusion flame burning concept. A one-dimensional problem for a burning solid fuel is defined, and the problem is solved based on conservation of species in stagnant layer and conservation of energy for the control volume at the surface of the fuel. Details of the solution to obtain burning rate of a fuel in a stagnant layer are explained in (Quintiere, 2006), and has the form of Eq. 26:

$$\dot{m}_{fuel}'' \approx \frac{h_c}{c_p} \ln(1+B) \quad \text{Eq. 26}$$

where the heat transfer coefficient h_c under turbulent condition can be assumed as 10 W/m²K, and c_p is the heat capacity of fuel (kJ/kgK). Parameter B is the Spaulding number and can be calculated using Eq. 27 when considering energy absorption by water.

$$B = \frac{Y_{O_2, \infty} (1 - X_{w,f}) \left(\frac{\Delta h_c}{r} \right) - c_p (T_v - T_\infty)}{L + \frac{\dot{m}_{water}'' L_w}{\dot{m}_{fuel}}} \quad \text{Eq. 27}$$

where $Y_{O_2, \infty}$ is the mass fraction of oxygen at the stagnant layer, $X_{w,f}$ is the relative value of absorbed energy by water over the flame energy, Δh_c is the heat of combustion of fuel (kJ/kg), r is the mass ratio of oxygen to fuel in stoichiometric reaction, T_v is the vaporization temperature (K), T_∞ is the ambient temperature with assumed value of 20°C (293 K), L is the effective heat of gasification of fuel (kJ/kg) (applies to steady

burning and non-charring material), \dot{m}_{fuel}'' is the mass loss rate of fuel per unit area (kg/m²), L_w is the heat of gasification of water (kJ/kg), and \dot{m}_{water}'' is the mass loss rate of water per unit area (kg/m²).

Meanwhile, extinction of a flame can be characterized by the flame temperature. The flame temperature can be related to the mass fraction of oxygen by solving the conservation of energy and species equations and defining mass loss rate of fuel (\dot{m}_{fuel}'') from Eq. 26 and Eq. 27:

$$c_p(T_f - T_\infty) = \frac{Y_{F,O}(1 - X_{w,f})(\Delta h_c) - \left(L + \frac{\dot{m}_{water}'' L_w}{\dot{m}_{fuel}''} \right) + c_p(T_v - T_\infty)}{1 + r \frac{Y_{F,O}}{Y_{O_2,\infty}}} \quad \text{Eq. 28}$$

where T_f is the temperature of the flame, $Y_{O_2,\infty}$ is the mass fraction of oxygen at the stagnant layer, and $Y_{F,O}$ is the concentration of fuel (equals to unit value for the condensed phase of fuel). Extinction of fire occurs by minimizing the rate of chemical reaction, removing the reactants, decreasing the temperature, or removing the source of flame. Fendell (1964) states that the rate of chemical reaction will enter the weak burning stage if the flame temperature reaches a critical temperature. Quintiere and Rangwala (2004) approximate the critical temperature as 1300°C (1573 K). Therefore, Eq. 28 provides the mass fraction of stagnant layer during extinction $Y_{O_2(extinction)}$ when T_f is substituted by the critical temperature.

Finally, the suppression time can be defined as the time that the mass fraction of oxygen in the system makes transition from the steady state condition ($Y_{O_2(ss)}$) to the oxygen fraction at extinction ($Y_{O_2(extinction)}$). Parameter $Y_{O_2(ss)}$ is the oxygen mass fraction at the time of suppression, and can be obtained by solving the equation of species. Back et al. (2000) relate the suppression time ($t_{extinction}$) to the oxygen fraction at the steady state and extinction conditions based on:

$$t_{extinction} = \ln \left(1 - \frac{Y_{O_2(extinction)}}{Y_{O_2(ss)}} \right) \left(\frac{-v}{\dot{v}} \right) \quad \text{Eq. 29}$$

where v is the volume of the fire compartment and \dot{v} is the volumetric flow rate of air in the system.

The mass fraction concentration of reactants and products in the stagnant layer of the control volume are a function of the type and quantity of fuel within the fire compartment. The type and quantity of fuel depends on the occupancy type of the building (e.g. residential, storage), and can be evaluated based on existing surveys and available data within literature. In this study, for an office occupancy, it is assumed that fuel consists of 67% wood/paper, 18% plastic, and 15% carpet (Ohlemiller et al., 2005). Details of the material compositions are provided in Table 6 with the corresponding molecular structure obtained from the ASTM E 2058 (ASTM, 2019).

Table 6: Assumed material compositions and molecular structure for fuel characterization

| Fuel type | Components | Molecular structure |
|-------------|------------------|-------------------------------------|
| Wood/ paper | Wood | CH _{1.7} O _{0.73} |
| | Polyethylene | CH ₂ |
| | Polypropylene | CH ₂ |
| Plastics | Polystyrene | CH |
| | Polystyrene foam | CH _{1.1} |
| | Polyester | CH _{1.4} O _{0.22} |
| Carpet | Polyester | CH _{1.4} O _{0.22} |

Considering an equal weight distribution for different plastics, and based on a weighted summation of wood, plastic, and textile, the obtained molecular structure for the lumped material becomes $\text{CH}_{1.6}\text{O}_{0.53}$. As a result, the fuel has heat of combustion of 18.3 kJ/kg, effective heat of evaporation of 1883.6 kJ/kg, and vaporization temperature of 402°C (675 K).

The objective is to calculate the fire extinguishing time for the defined compartment in Section 5.1.6 (with a size of 10 m × 10 m × 3 m, and HRR and temperature evolutions of Figure 6). Following the mathematical procedure briefly described in this section, the suppression time follows the histogram of Figure 8. For the purpose of minimizing the computational effort in the implemented framework, the suppression time is conservatively assumed as 10 minutes, which is towards the upper bound of the results. Future versions of the developed framework in this project will include more explicit calculation of the suppression process as a function of individual fire compartments.

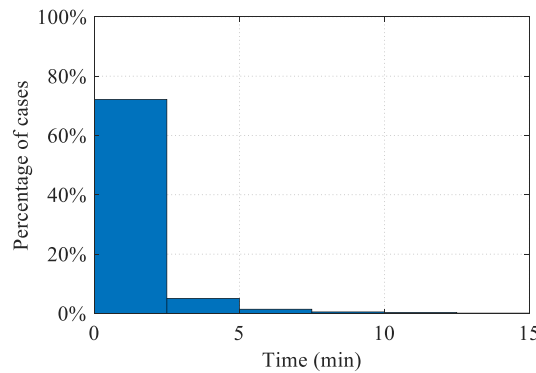


Figure 8: Histogram of suppression time for a compartment of 10 m × 10 m × 3 m with varying HRR and temperature defined in Figure 6

7 Decision-making algorithm for assignment of fire engines

Timely response of firefighters to the locations of ignition is crucial after an earthquake, as the community could sustain inevitable losses due to fire spread and conflagration. Damage to bridges and roadway blockage by building debris after an earthquake can degrade the operability of the transportation network and increase the response time of fire engines to the locations of ignition (Section 2). In addition, loss of functionality in the water network, due to direct damage to water network components (e.g., pipelines), or as a result of dependence on other lifelines (e.g., inoperability of pumps due to power loss), imposes a delay in fire suppression (Section 3).

A number of studies are available in the literature investigating algorithms for strategic pre-planning and efficient coordination of emergency responders to affected areas after natural disasters with the primary focus on decreasing the number of casualties (Marinov and Re Velle, 1996; Jia et al., 2007; Rawls and Turnquist, 2010; Noyan, 2012; Paul and Zhang, 2019). Management of resources during a disaster can be formulated in mathematical terms within a decision-making framework using an objective function. The objective function can be defined in terms of the maximum gain or the minimum loss. The objective of this section is to optimize fire engine assignments to locations of fire ignitions after an earthquake, such that the corresponding losses are minimized or the coverage value is maximized, considering damage to the transportation and water networks, as well as fire spread within and between buildings. This optimization problem becomes more critical when the number of ignitions (i.e., target points) outnumbers the available fire engines (i.e., resources). In this study, the optimization process is completed based on the appraised value of buildings that are damaged due to fire. The indirect economic losses (e.g., loss of business revenue) and number of casualties are not included in the calculation of losses.

7.1 Objective function

The decision-making process for fire engine assignment is divided into two steps: a) to allocate fire engines to locations of ignition, and b) to assign fire engines to fire compartments at a given specific ignition location. Fire engine assignments to locations of ignition are optimized, but once at a fire location, the fire engines are assigned to fires at higher stories of a building to control the vertical fire spread. A single objective function is defined as a Mixed-Integer Linear Programming (MILP) problem to decide on resource allocation to locations of ignition, as formulated in Eq. 30:

$$\max \sum_i \sum_j X_{ij}(C_j + T_{ij} + W_j), \forall i \in I, \forall j \in J \quad \text{Eq. 30}$$

$$C_j = \frac{c_j}{\sum_j c_j} \quad \text{Eq. 31}$$

$$T_{ij} = 1 - \frac{\min t_{ij}}{\sum_j t_{ij}} \quad \text{Eq. 32}$$

Subjected to the following static conditional constraints:

$$\text{if } m \geq n, \sum_j X_{ij} \geq 1, \forall j \in J \quad \text{Eq. 33}$$

$$\text{if } m < n, \sum_k X_{ik} \geq 1, \forall k \in K \quad \text{Eq. 34}$$

$$X_{ij} \in \{0, 1\} \quad \text{Eq. 35}$$

where, the input variables are defined as:

I : set of available fire engines

J : set of fire locations

m : total number of fire engines

n : number of fire locations

K : set of fire locations sorted based on the value of $C_k + W_{ik}$

c_j : coverage cost of building j

t_{ij} : travel time for fire engine i that is dispatched to building j

W_j : weighing coefficient indicating if the nearest hydrant in the water network has enough pressure or not

The decision variable is defined as:

X_{ij} : a binary variable with the value of 1 when fire engine i is assigned to building j , and 0 otherwise.

Eq. 30 maximizes the coverage cost and minimizes the travel time based on a weighted sum method. The parameter C_j is the normalized appraised value of building j with respect to the total appraised values of all buildings on fire as defined in Eq. 31. The input variable T_{ij} is the normalized response time, a parameter

to ensure that fire engines closer to the ignition locations receive priority compared to those with longer travel time.

The objective function is setup to be maximized, therefore, the variable T_{ij} is defined such that it results in a larger value when the fire location is within the service area of a fire engine, or is closer to the location of an ignition. The variable t_{ij} is the travel time for fire engine i from the current location to the ignition location j . The variable t_{ij} is calculated as the summation of the utilization time and the least travel time from the origin to destination based on the Dijkstra's shortest path algorithm (Section 2). The utilization time includes detection time, time to call and report the fire, coordination and resource assignment, and delay time due to preparation.

The coefficient W_j is an input from the water network analysis (Section 3) to determine whether the water pressure in the nearest water hydrant is sufficient to extinguish the fire (greater than 20 psi) or not. In case of sufficient water pressure, the coefficient W_j is assigned a value of 0, and in case of insufficient pressure, the coefficient W_j receives -1 (a negative value while compatible with the magnitude of other input variables).

The static conditional constraints of Eq. 33 and Eq. 34 ensure that at least one fire engine is assigned to each fire location. The first constraint (Eq. 33) applies when the number of fire engines (m) is higher than the number of fire locations (n), whereas the latter one (Eq. 34) applies to the opposite case. Eq. 34 assigns m fire engines to the locations of ignition that are sorted based on the highest values of $C_k + W_{ik}$. These constraints prevent concentration of all fire engines at one location (i.e., a building with large appraised value), especially for communities with a large dispersion in appraised building values. Finally, Eq. 35 is defined as a constraint for the input variable X to enforce a Boolean variable.

The single objective function in Eq. 30 is solved using the branch and bound algorithm. The branch and bound algorithm is an optimization scheme for non-convex problems that provides the global optimal values of the objective function within the designated bounds (Boyd and Vandenberghe, 2004). This method subdivides the original objective to several subproblems. The term *branching* refers to growing the problem and adding more constraint, where *bounding* prevents the unnecessary growth of the problem by putting a bound on the best solution and excluding subproblems that are not feasible or optimal.

7.2 Implementation of the objective function

The defined objective function in Section 7.1 is solved at each time step, while there is at least one available fire engine and an on-going fire in the community, to ensure a dynamic fire engine assignment throughout the analysis. In the implemented process, the model retrieves information about all buildings with ignition and keeps track of fire spread within the community (Sections 4 and 5). Locations of fire determine the possible destinations for available fire engines. The algorithm tracks the location of fire engines at each time step, where unavailable fire engines are designated as those that are assigned to a fire location and have not reached the destination (tracked based on the result of transportation network in Section 2), or those that are active suppressing a fire. Losses, in terms of appraised value of damaged buildings, are reported as an output.

8 Application to a case study

The developed framework is applied to a case study. This section provides an overview of inputs to the model, organization of data, and the obtained results. The area of study is a densely populated area located on the West coast of the US. The selected area covers 6 census tracts and a total of about 600 buildings. Table 7 lists the building type, population density, and total floor area of buildings included in the analysis. Note that 9 additional buildings are included from nearby census tracts in the transportation analysis to account for possible roadway blockage (these buildings are shown with a hashed pattern in Figure 9a).

Table 7: Description of census tracts for the case study

| Census tract ID | Building type | | Population density (people per km ²) | Floor area (m ²) |
|--------------------|---------------|----------------|---|---------------------------------|
| | Wood | Noncombustible | | |
| 72 | 15 | 105 | 7.9E+03 | 5.7E+05 |
| 73 | 9 | 58 | 6.4E+03 | 6.5E+05 |
| 80.01 | 22 | 80 | 13.0E+03 | 3.5E+05 |
| 80.02 | 14 | 76 | 15.0E+03 | 3.2E+05 |
| 81 | 9 | 167 | 5.6E+03 | 1.9E+06 |
| 82 | 1 | 36 | 11.0E+03 | 8.3E+05 |
| Other | - | 9 | - | - |
| Total | 70 | 531 | - | - |

Figure 9 categorizes the building data with respect to census tracks, height, year of construction, and construction type. The majority of buildings are noncombustible (steel, concrete, and masonry), and are constructed post-1974. The presented information in Table 7 and Figure 9 are inputs to calculate debris width, probability of ignition, and the fire spread. The three-dimensional layout of the case study is constructed and presented in Figure 10, where each fire compartment is defined as 10 m \times 10 m \times 3 m with an associated fire behavior.

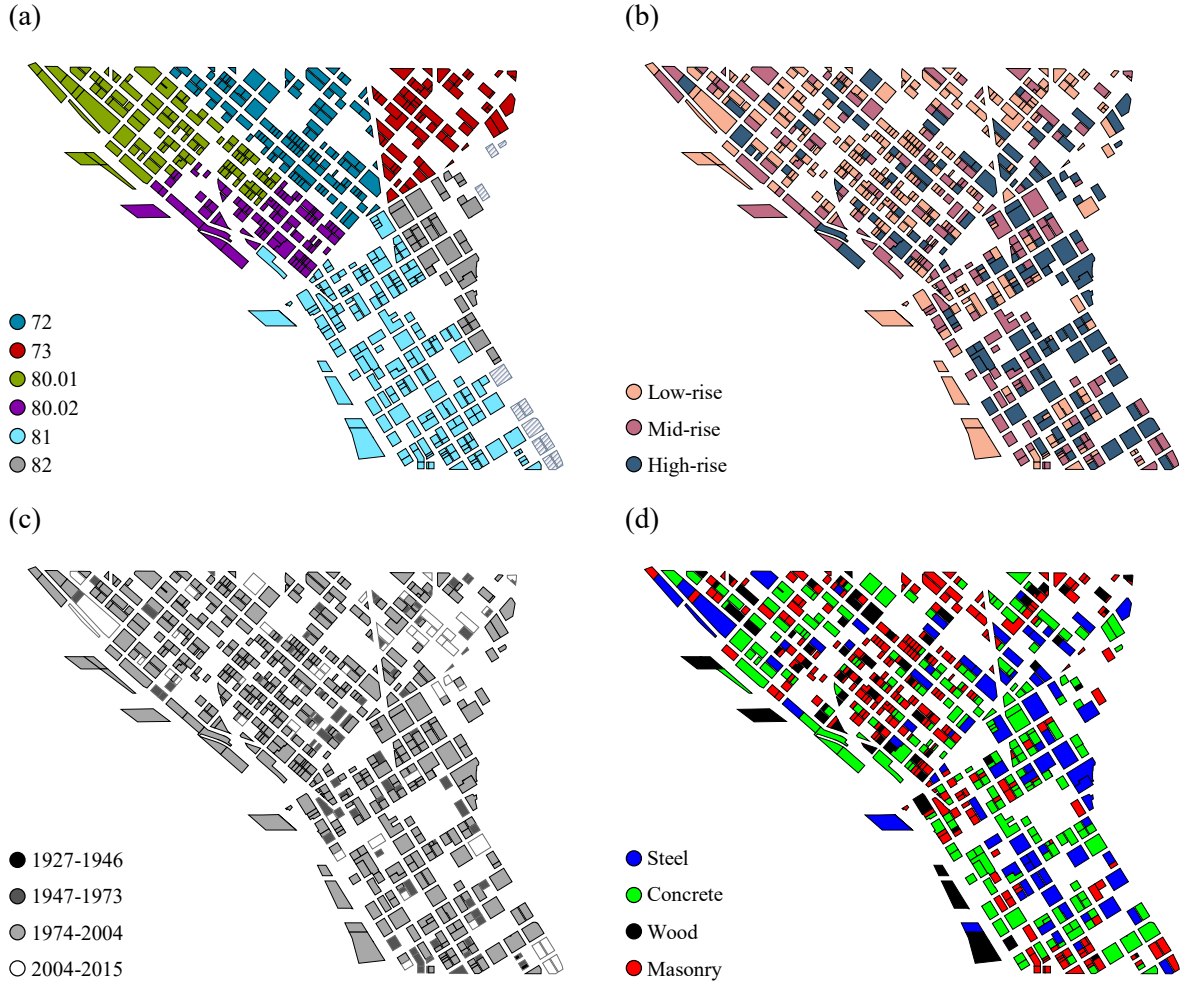


Figure 9: Building data for the case study categorized based on (a) census tract number, (b) building height, (c) year of construction, and (d) construction type

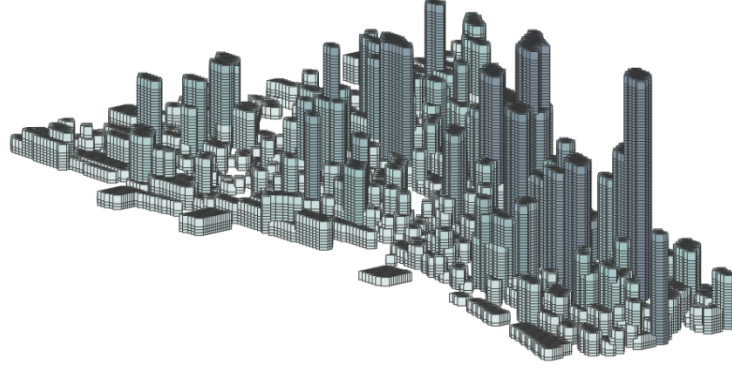


Figure 10: Three-dimensional layout of buildings in the case study

Figure 11 shows the probability of ignition for each census tract, and two examples for *PGA* values of 0.4 and 0.7 g, based on the procedure described in Section 4. The likelihood of ignition is highest in census tract 81, where the total floor area of buildings is considerably larger compared to other census tracts. The probability of ignition at a census tract can be mapped to individual buildings based on their construction type, which is of benefit for a weighted random assignment of ignitions to buildings in the community, and estimation of the total probable number of ignitions. The total number of ignitions across the community for *PGAs* of 0.4 g and 0.7 are 1 and 9, respectively. Once a building location is determined to have an ignition, the compartment at which the fire starts inside the building is selected randomly with a uniform distribution.

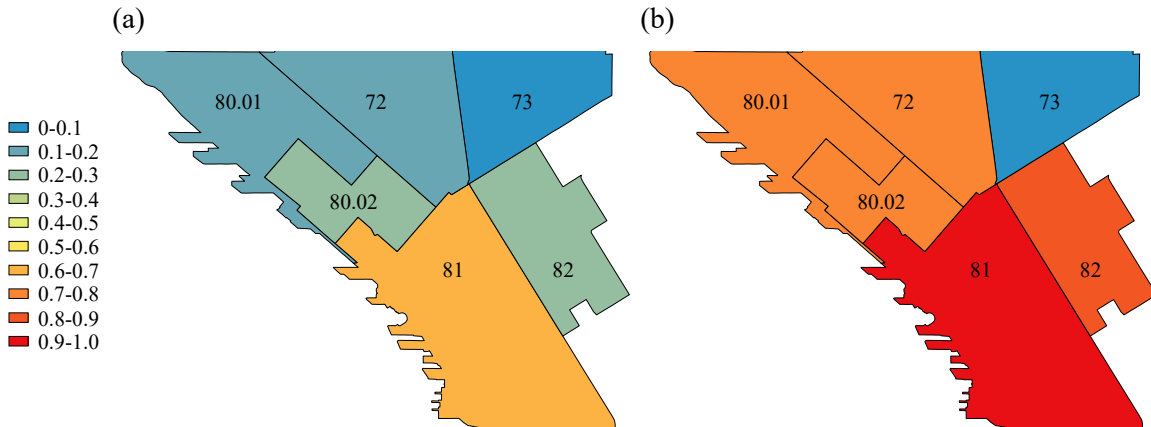


Figure 11: Probability contours of ignition in census tracts for *PGA* values of (a) 0.4 g, (b) 0.7 g.

The transportation network for the area of study (Figure 12a) includes 515 roadways with assigned number of lanes, speed limit, and a curb width of 3.5 m (12 ft). There are a number of bridges located on the boundaries of the study area, but they do not affect the response time of fire departments within the area of study and are therefore excluded from the analyses. Two fire stations, one with 3 fire engines and one with 4 fire engines, are located in north and south west of the area, as labeled in Figure 12a. It is assumed that each fire engine is capable of suppressing a fire without relying on other fire engines. As discussed in Section 7, the total response time of firefighters is the summation of travel time, calculated based on roadway accessibility, and a utilization time.

The water network, shown in Figure 12b, includes three reservoirs located at north, east, and south of the community. The network for the considered area is gravity driven and thus no pumps are utilized in the model, making the water network independent of power for functionality after an earthquake. Performance analysis of the water network concluded with a robust system within the area of study, providing enough pressure for firefighting actions 14 m (20 psi) while assuming that water supply from outside of the considered boundaries are not significantly affected due to earthquake damage (analysis of components outside of the defined boundaries are outside of the scope of this case study).

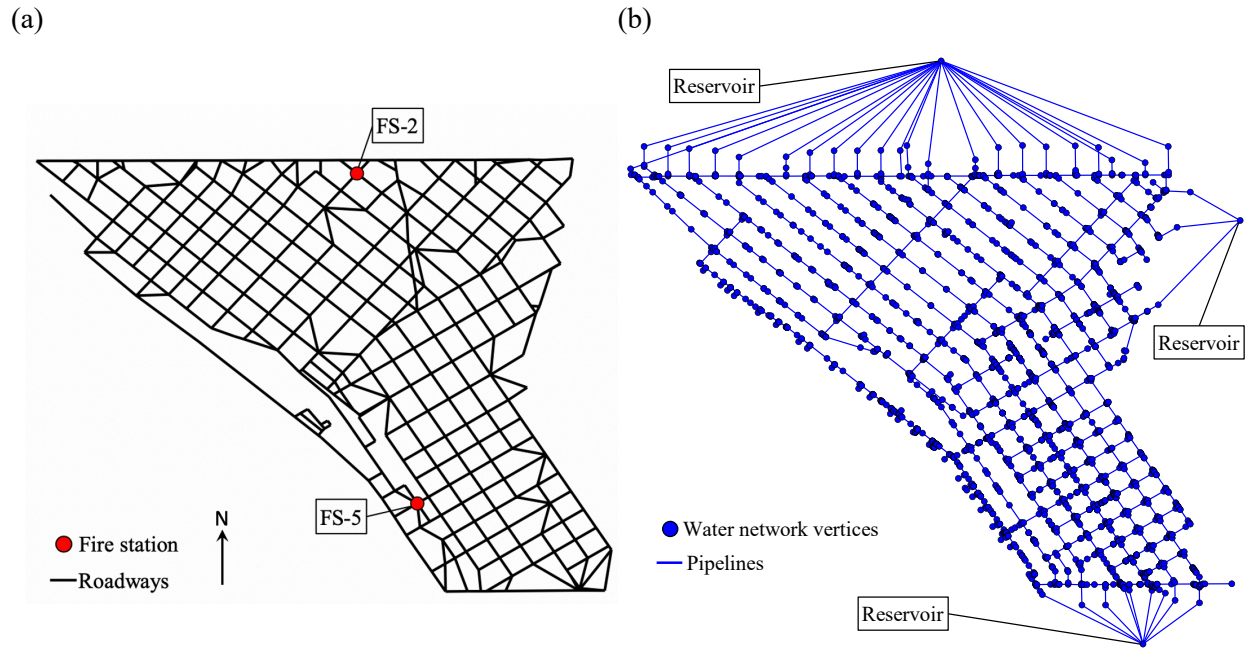


Figure 12: (a) Transportation network and locations of fire departments, and (b) water network for the area of study

The analysis is completed by performing 70 iterations to consider uncertainty in random variables, as previously discussed in this report. The number of iterations is selected based on convergence checks. The total analysis time, to track fire spread and suppression activities, is set to 500 minutes (8 hours and 20 minutes), with a 5-minute time step. Sample of results are provided for a case with an average wind speed of 6 m/s and wind direction of 190 degrees from east in counter clockwise direction. Community response to FFE is reported using two criteria: (1) induced economic losses due to fire, and (2) whether or not the suppression actions by fire departments are successful and fire ignitions are contained. Simulated cases with a *successful suppression*, where the fire departments manage to stop fire propagation, are typically those with relatively low number of fire ignitions and when roadway accessibility is not compromised for the fire department response. Simulated cases with *unsuccessful suppression*, where fire spread is out of control, typically occurs when the number of fire ignitions exceed the number of available fire engines, and when blocked roadways create inaccessible islands within the transportation network.

Reported losses are based on the appraised value of buildings and the number of compartments damaged by fire. Losses can be minor if the fire is controlled at early stages of ignition or can be significant when first responders are overwhelmed by the level of demand and fire spread becomes out of control. Figure 13 shows the cumulative economic losses over time for 70 iterations and for scenarios with *PGA* values of 0.4g and 0.7g. All iterations for *PGA* of 0.4 g are successfully suppressed, as there is only one ignition involved and damage to the transportation network is minor. The total loss is a function of the initial location of ignition with the mean value of about \$0.6 million. The area of study experiences much larger losses for

the case of 0.7 g. Results of 70 iterations show a mix of cases with successful and unsuccessful suppression (shown in Figure 13b). The rate of increase in losses vary among the unsuccessful cases, with a number of cases showing an exponential trend (labeled as extreme cases in Figure 13b). The extreme cases experience ignitions within buildings with high appraised value and an out-of-control fire spread.

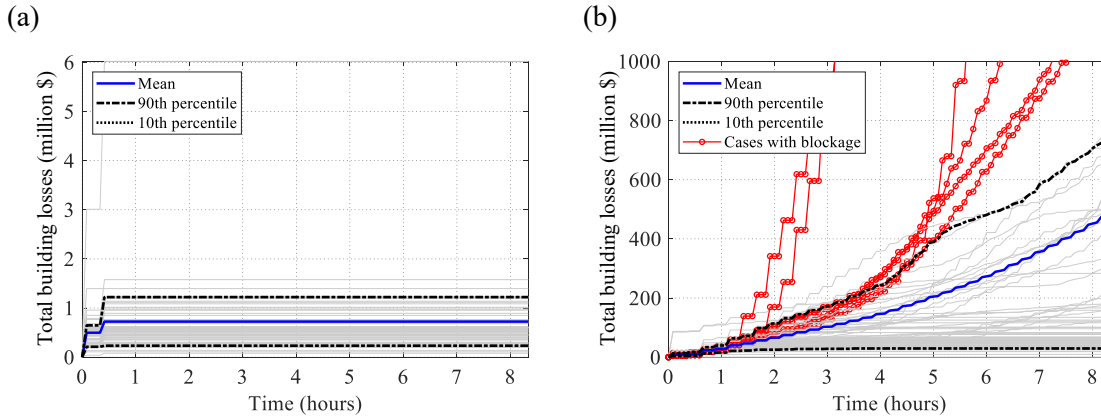


Figure 13: Total building losses over time for PGA values of (a) 0.4g and (b) 0.7g

Figure 14 and Figure 15 show details of two cases for PGA of 0.7 g with the same number of ignitions but successful and unsuccessful suppressions, respectively. Figure 14a shows the randomly generated 9 locations of ignition, and Figure 14b provides the final extent of fire propagation, which is controlled by successful suppression. Figure 14c shows the level of damage to the transportation network, including partial (represented by faded edges) and complete blockage (represented by elimination of an edge) of the roadways. Fire engines reach the locations of fire; either by selecting the same route as the intact condition, accepting the penalty of increase in travel time or detouring to bypass locations with complete blockage. Figure 14d reports evolution of fire in the community with respect to time. The number of fire engines (in this case 7) is less than the number of ignitions, thus, assignment of fire engines to locations of ignition are determined based on the optimization algorithm to minimize losses. At time t_a (Figure 14d), fire engines reach locations of ignition and start the suppression action. The active number of fires keep increasing until about 2 hours, as the rate of suppression becomes larger than fire spread rate, until a complete confinement of fire is reached at time t_b . Figure 14d also shows the accumulated active, burnt, and suppressed areas, where a burnt area is a compartment that fire is out (i.e., fuel is completely burnt) but without response from the fire department. Figure 15 shows similar results but for a case with unsuccessful suppression, where the rate of fire spread at early stages of analysis is beyond capabilities of fire fighters and the rate of fire spread exceeds the suppression rate. The difference between the two cases are the initial locations of ignition, which changes the amount of fuel and fire behavior in the initial fire compartment, as well as damage to the transportation network. The initial locations of ignitions and fire behavior in the compartment could lead to fires with higher temperatures, for which spread is more probable, while the layout of surrounding buildings could also contribute to a faster spread rate.

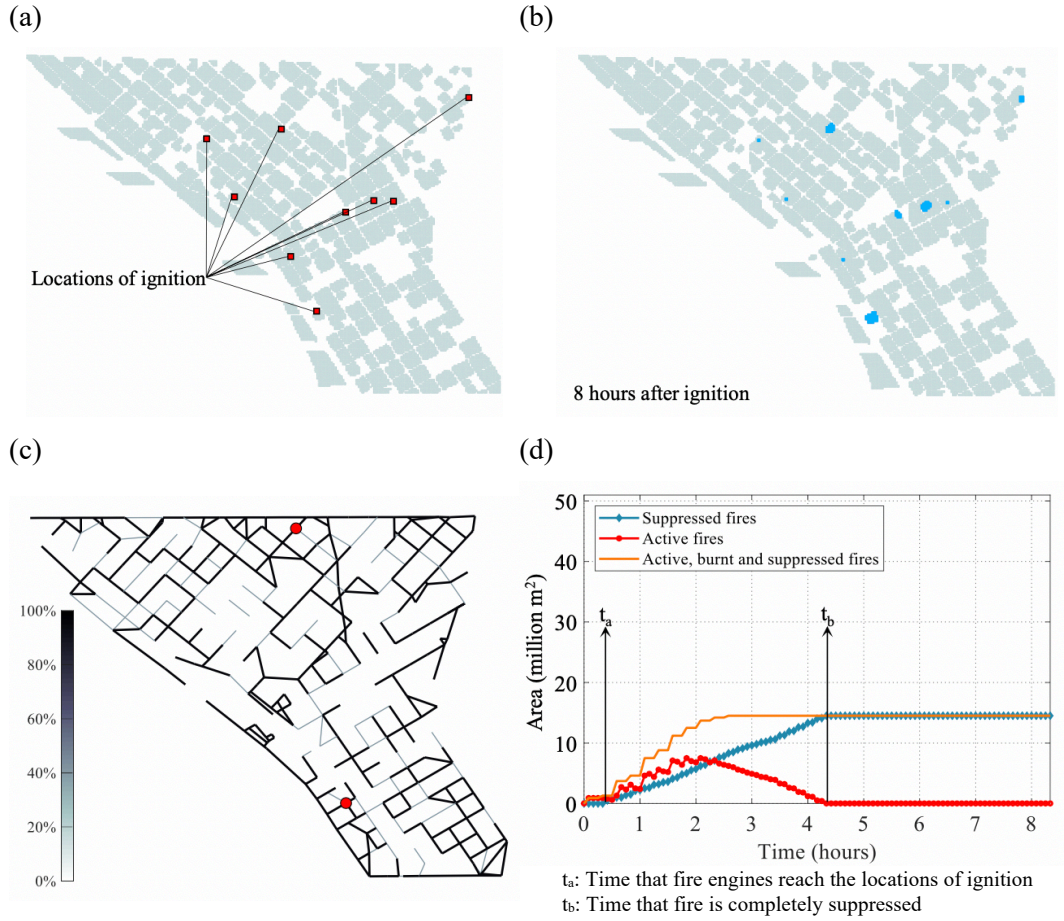


Figure 14: Example of successful suppression for PGA of 0.7 g: (a) locations of ignition, (b) extent of fire spread in the community, (c) damaged transportation network, and (d) evolution of fire spread and suppression actions over time in terms of affected area

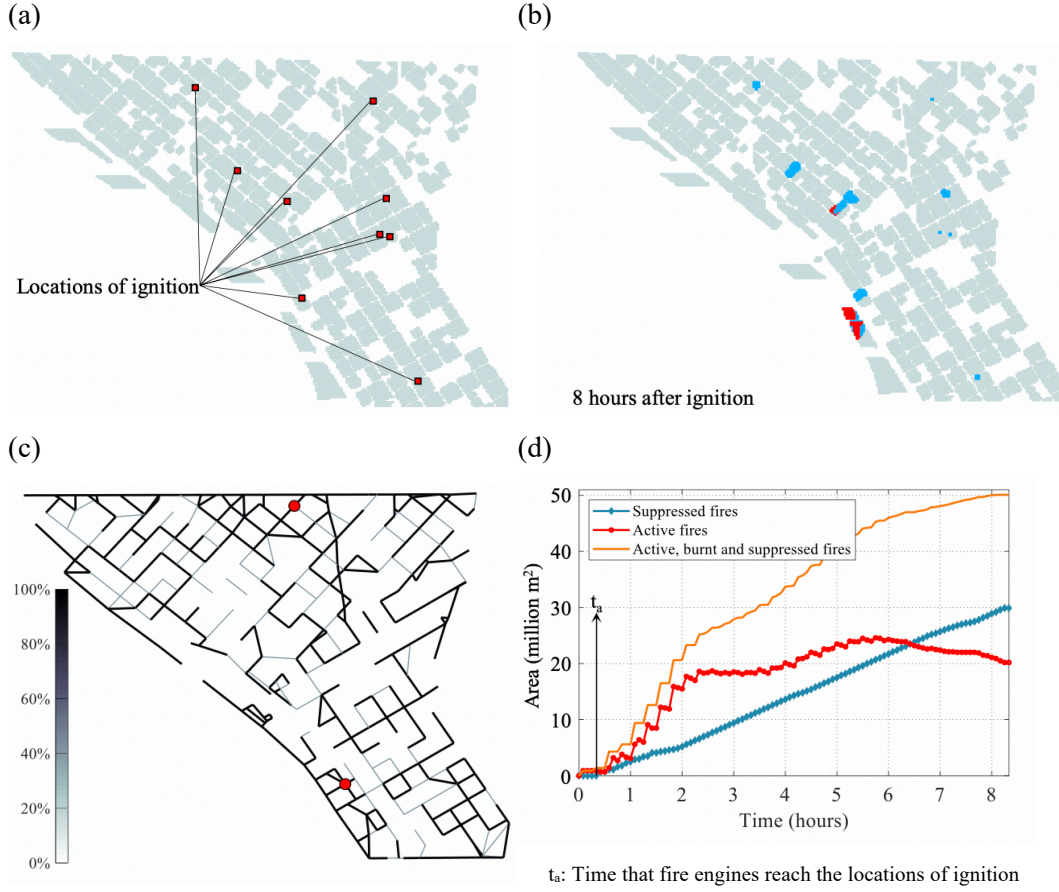


Figure 15: Example of unsuccessful suppression for PGA of 0.7 g: (a) locations of ignition, (b) extent of fire spread in the community, (c) damaged transportation network, and (d) evolution of fire spread and suppression actions over time in terms of affected area

Finally, response of the community is characterized by the likelihood of unsuccessful suppression as a function of PGA . Figure 16 shows the fragility function for the exceedance of unsuccessful suppression action, and the tipping point for this community is identified as PGA of 0.7 g where the probability of out-of-control fires become significantly larger. The number of ignitions within the community changes from 7 to 9 when PGA changes from 0.6 to 0.7 g.

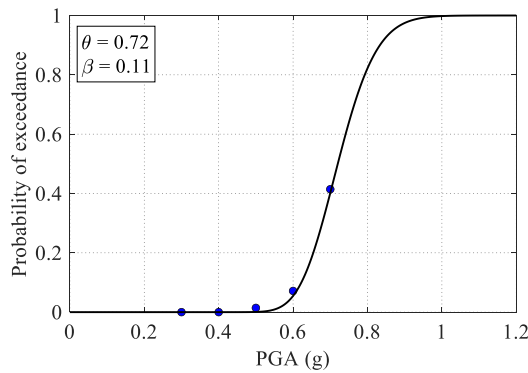


Figure 16: Fragility curve for the exceedance of unsuccessful suppression action

9 Conclusions

This report presented a framework to model and plan for impacts of FFE in an urban community. The framework captures damage to layers of infrastructure, including buildings, transportation network, electric network, water network, and their interaction, while taking into account fire spread behavior and suppression action by the fire department. Building and roadway layouts were explicitly modeled, and behavior of fire spread between building compartments were incorporated in the analysis. The model integrated different modes of fire spread (radiation, plume, direct contact, and fire branding), and varied temperature-time evolution and amount of fuel energy within building compartments. Assignment of fire engines for fire suppression was processed through a decision-making algorithm by considering appraised values of buildings and changes in response time and water pressure. Given the level of uncertainty in the procedure, the framework relied on stochastic quantification of earthquake damage and simulation of fire behavior.

Application to a case study demonstrated the importance of planning for FFE, and how fire can spread beyond control, leading to significant losses. A community tipping point can be identified as the earthquake intensity beyond which the number of ignitions, combined with damage to the infrastructure, makes suppression actions insufficient and ineffective. The rate of fire spread in such scenarios is beyond capacity of the fire department to confine the fire ignitions. Another key point is related to the assignment of fire engines, especially when the number of fire ignitions are larger than available resources. Proper and informed assignment of engines can lead to successful suppression of fires and reduced economic losses. In addition, redundancy in the transportation and water networks are needed to ensure effective fire department response, otherwise, lack of suppression action at early stages of fire can cause the fire to spread beyond control. The developed framework in this project reduced the epistemic uncertainty in predicting losses and risk estimates from FFE, which helps with mitigation, preparedness, and response planning.

10 Presentations and publications

- Sarreshtehdari, A., Elhami-Khorasani, N. (2019). *Emergency response time during post-earthquake fires*, abstract and presentation at the Engineering Mechanics Institute Conference, Pasadena, CA, June 18-21.
- Sarreshtehdari, A., Elhami-Khorasani, N. (2020). "Post-earthquake emergency response time to locations of fire ignition," *Journal of Earthquake Engineering*, 10.1080/13632469.2020.1802369.
- Sarreshtehdari, A., Coar, M., Elhami-Khorasani, N. (2021). "Planning for post-earthquake fires considering performance of transportation and water networks," *Proceedings of the ASCE Lifelines Conference*, University of California, Los Angeles, CA.
- Sarreshtehdari, A., Elhami-Khorasani, N. "A decision-making framework for managing fire following earthquake losses," To be submitted to *Fire Safety Journal*.

11 Project data

- Source code for the fragility function tool (Figure 2) and a demo (in the form of a video) will be publicly available at: <https://github.com/amirsarr/FFEPProject/tree/master/FCUI>
- A demo (in the form of a video) of the implemented framework will be publicly available at: <https://github.com/amirsarr/FFEPProject/tree/master/DecisionMaking>

12 References

- Adachi, T., and Ellingwood, B. R. (2008). "Serviceability of earthquake-damaged water systems: Effects of electrical power availability and power backup systems on system vulnerability." *Reliability Engineering & System Safety*, 93(1), 78–88.
- Alexoudi, M., Pitilakis, K., Souli, A. (2010). *Fragility functions for water and waste-water system elements*, SYNER-G D3.5, Aristotle University of Thessaloniki, Greece.

- Anshel J. S. (1985). "The Morgan Hill Earthquake of April 24, 1984—Investigation of Lifelines." *Earthquake Spectra*, 1(3), 615-632.
- Anthenien, R. A., Tse, S. D., Carlos Fernandez-Pello, A. (2006). "On the trajectories of embers initially elevated or lofted by small scale ground fire plumes in high winds." *Fire Safety Journal*, 41(5), 349–363.
- Argyroudis, S., Selva, J., Gehl, P. (2015). "Systemic Seismic Risk Assessment of Road Networks Considering Interactions with the Built Environment." *Computer-Aided Civil and Infrastructure Engineering*, 30, 524-540.
- ASTM E 2058. (2019). "Standard test methods for measurement of material flammability using a fire propagation apparatus (FPA)." *American Society for Testing and Materials*, West Conshohocken, Pennsylvania.
- Atkins, K., Chen, J., Kumar, V.S.A., Marathe, A. (2009). "The structure of electrical networks: a graph theory-based analysis." *International Journal of Critical Infrastructures*, 5(3), 265-284.
- Back III, G. G., Beyler, C. L., Hansen, R. (2000). "A quasi-steady-state model for predicting fire suppression in spaces protected by water mist systems." *Fire Safety Journal*, 35(4), 327–362.
- Bai, J. W., Hueste, M. B. D., and Gardoni, P. (2009). "Probabilistic assessment of structural damage due to earthquakes for buildings in Mid-America." *Journal of Structural Engineering*, 135(10), 1155-1163.
- Bailey, C. G., Burgess, I. W., Plank, R. J. (1996). "Analyses of the effects of cooling and fire spread on steel-framed buildings." *Fire Safety Journal*, 26(4), 273–293.
- Beyler, C. L. (1986). "Fire plumes and ceiling jets." *Fire Safety Journal*, 11(1), 53–75.
- Boonmee, N. (2004) "Theoretical and experimental study of the auto-ignition of wood." PhD dissertation, Department of Fire Protection Engineering, University of Maryland, College Park, MD.
- Botting, R. (1998). *Impact of post-earthquake fire on the built environment*. Dissertation for M.E. (Fire) at the University of Canterbury, Christchurch, New Zealand.
- Boulos, P., Lansey, K., and Karney, B. (2004). *Comprehensive water distribution systems analysis*. Handbook for Engineers and Planners. 2nd edition, Pasadena, CA.
- Boyd, S., Vandenberghe, L. (2004) *Convex Optimization*, Cambridge University Press, United Kingdom.
- Boykov, Y., Kolmogorov, V. (2004). "An experimental comparison of min-cut/max-flow algorithms for energy minimization in vision." *IEEE Transactions on Pattern Analysis and Machine Intelligence* 26 (9), 1124–37.
- Cadorin, J.F., Franssen, J.M. (2003). "A tool to design steel elements submitted to compartment fires—OZone V2. Part 1: pre-and post-flashover compartment fire model" *Fire Safety Journal*, 38 (5), 395–427.
- Center for Computational Research. (2020). University at Buffalo, <http://hdl.handle.net/10477/79221>.
- Coar, M., Garlock, M., and Elhami Khorasani, N. (2020). "Effects of water network dependency on the electric network for post-earthquake fire suppression." *Sustainable and Resilient Infrastructure*, 5(5), <https://doi.org/10.1080/23789689.2018.1563408>
- Cousins, J., Heron, D., Mazzoni, S., Thomas, G., and Lloyd, D. (2002). *Estimating risks from fire following earthquake*, Institute of Geological & Nuclear Sciences client report 2002/60, New Zealand.
- Davidson, R. (2009). *Generalized linear (mixed) models of post-earthquake fire ignitions*. Technical Report MCEER-09-2004. Multidisciplinary Center for Earthquake Engineering Research, Buffalo.
- Davis, C.A., O'Rourke, T.D., Adams, M.I., Rho, M.A. (2012). "Case Study: Los Angeles Water Services Restoration Following the 1994 Northridge Earthquake." *Proceedings of the 15th World Conference on Earthquake Engineering*, Lisbon, Portugal.

- Deo, N. (1974). *Graph theory with applications to engineering and computer science*. Prentice-Hall, Inc., Upper Saddle River, NJ.
- Dijkstra, E. W. (1959). "A Note on Two Problems in Connexion with Graphs" *Numerische Mathematik*, 1(1).
- DOE. (2013). *Comparing the impacts of northeast hurricanes on energy infrastructure*. Office of Electricity Delivery and Energy Reliability U.S. Department of Energy.
- Drysdale, D. (2011). *An introduction to fire dynamics*. John Wiley & Sons Ltd., UK.
- Dueñas-Osorio, L., Craig, J. I., and Goodno, B. J. (2007). "Seismic response of critical interdependent networks." *Earthquake Engineering & Structural Dynamics*, John Wiley & Sons, Ltd, 36(2), 285–306.
- Elhami Khorasani, N., Gernay, T., and Garlock, M. (2017). "Data-driven probabilistic post-earthquake fire ignition model for a community." *Fire Safety Journal*, 94, 33–44.
- FEMA. (1991). *High-rise office building fire One Meridian Plaza Philadelphia, Pennsylvania*, Federal emergency management agency & United States Fire Administration, Washington, DC.
- FEMA. (2014). *Hazus: MH 2.1 technical manual - earthquake model*, developed by the department of homeland security. Federal emergency management agency. Mitigation Division, Washington, DC.
- Fendell, F.E., (1965). "Ignition and extinction in combustion of initially unmixed reactants". *Journal of Fluid Mechanics*, 21(2), 281–304.
- Fletcher, I.A., Borg, A., Hitchen, N., Welch, S.M. (2006). "Performance of concrete in fire: a review of the state of the art, with a case study of the Windsor tower fire." In *Proc., 4th Int. workshop on Structures in fire*, Aviero, Portugal.
- Franchin, P. (2014). "A Computational framework for systemic seismic risk analysis of civil infrastructural systems." *Geotechnical, Geological and Earthquake Engineering*, 31, 23–56.
- Gol'dshleger, U. I., Pribytkova, K. V, Barzykin, V. V. (1973). "Ignition of a condensed explosive by a hot object of finite dimensions." *Combustion, Explosion and Shock Waves*, 9(1), 99–102.
- Guillaume, E., Dréan, V., Girardin, B., Benameur, F., Fateh, T. (2020). "Reconstruction of Grenfell Tower fire. Part 1: Lessons from observations and determination of work hypotheses." *Fire and Materials*, John Wiley & Sons, Ltd, 44(1), 3–14.
- Himoto, K., Tanaka, T. (2002). "A physically-based model for urban fire spread." *International Association for Fire Safety Science*, 129–140.
- Himoto, K. Tanaka, T. (2005), "Transport of disk-shaped firebrands in a turbulent boundary layer." *Fire Safety Science*, 8: 433-444.
- Himoto, K., Tanaka, T. (2012). "A model for the fire-fighting activity of local residents in urban fires." *Fire Safety Journal*, 54, 154–166.
- Iwami, T., Ohmiya, Y., Hayashi, Y., Kagiya, K., Takahashi, W., Naruse, T.N. (2004). "Simulation of city fire." *Fire Science and Technology*, 23(2): 132–140.
- Jia, H., Ordóñez, F., and Dessouky, M. M. (2007). "Solution approaches for facility location of medical supplies for large-scale emergencies." *Computers & Industrial Engineering*, 52(2), 257–276.
- Johnson L.A., Mahin, S.A. (2016). "The Mw 6.0 South Napa Earthquake of August 24, 2014: A Wake-up Call for Renewed Investment in Seismic Resilience across California." California Seismic Safety Commission, Pacific Earthquake Engineering Research Center (PEER), CSSC Publication 16- 03, PEER Report No. 2016/04.

- Lee, S., Davidson, R. (2010a). "Application of a physics-based simulation model to examine post-earthquake fire spread." *Journal of Earthquake Engineering*, 14(5): 688–705.
- Lee, S., Davidson, R. (2010b). "Physics-based simulation model of post-earthquake fire spread." *Journal of Earthquake Engineering*, 14(5): 670–687.
- Li, S., Davidson, R. (2013). "Application of an urban fire simulation model." *Earthquake Spectra*, 29 (4): 1–21.
- MAEViz. (2014). Hosted by the National Center for Supercomputing Applications, at the University of Illinois, Urbana: <https://wiki.ncsa.illinois.edu/display/MAE/Home>
- McAllister, T. P., Gross, J. L., Sadek, F., Kirkpatrick, S., MacNeill, R. A., Zarghamee, M., Erbay, O. O., Sarawit, A. T. (2013). "Structural response of World Trade Center Buildings 1, 2 and 7 to impact and fire damage." *Fire Technology*, 49(3), 709–739.
- MFB. (2014). *Post incident analysis report: Lacrosse Docklands*, Melbourne Metropolitan Fire and Emergency Services Board, Melbourne, Australia.
- Noyan, N. (2012). "Risk-averse two-stage stochastic programming with an application to disaster management." *Computers & Operations Research*, 39(3), 541–559.
- Nussle, T., Kleiner, A., Brenner, M. (2004). *Approaching urban disaster reality: The ResQ Fire simulator*. <http://www.science.uva.nl/~arnoud/research/roboresc/robocup2004/tdps-Rescue-Simulation-2004/01.PDF>
- NYCEM: The New York City Area Consortium for Earthquake Loss Mitigation. (2003). *Earthquake Risks and Mitigation in the New York, New Jersey, Connecticut Region*. Report Number MCEER-03- SP02.
- Ohmiya, F. Iwami, T. (2000). "An investigation on the distribution of fire brands and spot fires due to a hotel fire." *Fire Science and Technology*, 20(1); 27–35
- Otake, H., Huang, H., Ooka, Y., Kato, S., Hayashi, Y. (2003). "Simulation of flames and thermal plume in urban fire under windy condition." *Proceedings of the 17th Japan Society of Fluid Mechanics Symposium*, paper E.2-2 (In Japanese).
- Paul, J. A., Zhang, M. (2019). "Supply location and transportation planning for hurricanes: A two-stage stochastic programming framework." *European Journal of Operational Research*, 274(1), 108–125.
- Quintiere, J.G. Rangwala, A.S., (2004). "A theory for flame extinction based on flame temperature" *Fire and Materials*, 28, 387–402.
- Quintiere, J. G. (2006). *Fundamentals of Fire Phenomena*. John Wiley & Sons Ltd., UK.
- Rackauskaite, E., Kotsovinos, P., and Rein, G. (2017). "Structural response of a steel-frame building to horizontal and vertical travelling fires in multiple floors." *Fire Safety Journal*, 91, 542–552.
- Rafi, M. M., Aziz, T., Lodi, S. H. (2020). "A suggested model for mass fire spread." *Sustainable and Resilient Infrastructure*, Taylor & Francis, 5(4), 214–231.
- Rawls, C. G., Turnquist, M. A. (2010). "Pre-positioning of emergency supplies for disaster response." *Transportation Research Part B: Methodological*, 44(4), 521–534.
- Röben, C., Gillie, M., Torero, J. (2010). "Structural behaviour during a vertically travelling fire." *Journal of Constructional Steel Research*, 66(2), 191–197.
- Rehm, R., Pitts, W., Baum, H., Evans, D., Prasad, K., Mcgrattan, K., Forney, G. (2003). "Initial model for fires in the World Trade Center Towers." *Fire Safety Science*, 7.
- Sardoy, N., Consalvi, J.-L., Porterie, B., Fernandez-Pello, A.C. (2007). "Modeling transport and combustion of firebrands from burning trees." *Combustion and Flame*, 150(3), 151–169.

- Sarreshtehdari, A., Elhami Khorasani, N., Coar, M. (2020). “A streamlined approach for evaluating post-earthquake performance of an electric network.” *Sustainable and Resilient Infrastructure*, 5(4).
- Sarreshtehdari, A., Elhami-Khorasani, N. (2020). “Post-earthquake emergency response time to locations of fire ignition”, *Journal of Earthquake Engineering*, in press, 10.1080/13632469.2020.1802369.
- Scawthorn, C.R., Yamada, Y., Iemura, H. (1981). “A model for urban post-earthquake fire hazard.” *Disasters*, England, 5(2), 125–132.
- Scawthorn, C.R., Bureau, G., Jessup, C., Delgado, R. (1985). “The Morgan Hill earthquake of April 24, 1984—Fire-related aspects.” *Earthquake Spectra*, SAGE Publications Ltd STM, 1(3), 675–685.
- Scawthorn, C.R., Eidinger, J. M., Schiff, A.J. (2005). *Fire Following Earthquake*. American Society of Civil Engineers.
- Scawthorn, C.R. (2008). *The ShakeOut Scenario – Fire Following Earthquake*, Prepared for United States Geological Survey, Pasadena, CA and California Geological Survey, Sacramento, CA.
- Scawthorn, C.R. (2019). *Fire following earthquake in Montreal region*, Prepared for the Institute for Catastrophic Loss Reduction, ICLR research paper series 63, Toronto, Ontario, Canada.
- Schiff, A.J. (1998). *The Loma Prieta, California, Earthquake of October 17, 1989: Lifelines*. U.S. Geological Survey Professional Paper 1552-A, Washington: U.S. G.P.O.
- Spearpoint, M.J. (1999). *Predicting the ignition and burning rate of wood in the cone calorimeter using an integral model*. MS thesis, Department of Fire Protection Engineering, University of Maryland, College Park, MD.
- Shi, P., O’Rourke, T. D. (2008). *Seismic response modeling of water supply systems*, Technical Report MCEER-08-0016, Buffalo, NY.
- Shinozuka, M. (1995). *The Hanshin-Awaji earthquake of January 17, 1995: performance of lifelines*. Technical Report NCEER-95-0015, Buffalo, NY.
- Shinozuka, M., Rose, A., Eguchi, R.T. (1998). *Engineering and socioeconomic impacts of earthquakes: An analysis of electricity lifeline disruptions in the New Madrid area*, Technical report MCEER, Buffalo, NY.
- Shinozuka, M., Chang, S.E., Cheng, T.C., Feng, M., O’Rourke, T.D., Saadeghvaziri, M.A., Dong, X., Jin, X., Wang, Y., Shi, P. (2004). *Resilience of integrated power and water systems*. MCEER Research Progress and Accomplishments, 65-86.
- Tanaka, T. (2016). “Vent Flows.” *SFPE Handbook of Fire Protection Engineering*, M. J. Hurley, D. Gottuk, J. R. Hall, K. Harada, E. Kuligowski, M. Puchovsky, J. Torero, J. M. Watts, and C. Wieczorek, NY: Springer New York, 455–485.
- Tokyo Fire Department. (1997). *Determinations and measures on the causes of new fire occurrence and properties of fire spreading on an earthquake with a vertical shock (in Japanese)*. Prevention Deliberation Council Report, Tokyo, Japan.
- Verriopoulos, P. A., Papailiou, D. D. (1994). “Structure of the Turbulent Temperature Field of a Two-Dimensional Fire Plume.” *Progress in Turbulence Research*, Progress in Astronautics and Aeronautics, H. Branover and Y. Unger, eds., American Institute of Aeronautics and Astronautics, 218–236.
- Waterman, T. (1969). *Experimental study of firebrand generation*, IIT Research Institute, Project J6130, Chicago, IL.
- Waterman, T., Takata, A. (1969). *Laboratory study of ignition of host materials by firebrands*, IIT Research Institute, Project J6142, Chicago, IL.

- Wellington Lifelines Group. (2002), *Fire following earthquake: identifying key issues for New Zealand*, The New Zealand Fire Service Contestable Research Fund, Wellington, New Zealand.
- Woycheese, J. P., Pagni, P. J., and Liepmann, D. (1999). "Brand propagation from large-scale fires," *Journal of Fire Protection Engineering*, SAGE Publications Ltd STM, 10(2), 32–44.
- Yang, S. C., Liu, T. J. and Hong, H. P. (2017). "Reliability of tower and tower-line systems under spatiotemporally varying wind or earthquake loads." *Journal of Structural Engineering*, 143(10), 1–13.
- Yildiz, S.S., Karaman, H. (2013). "Post-earthquake ignition vulnerability assessment of Kucukcekmece District". *Journal of Natural Hazards and Earth System Sciences*. 13, 3357-3368.
- Zhao, S. (2010). "GisFFE—an integrated software system for the dynamic simulation of fires following an earthquake based on GIS." *Fire Safety Journal*, 45(2), 83–97.